Targeted Delivery of Letrozole-loaded Mg-doped Cobalt Ferrite Nanoparticles for Breast Cancer Treatment

By

Huma Ijaz

(Registration No: 00000402052)

Department of Materials Engineering

School of Chemical and Materials Engineering

National University of Sciences & Technology (NUST)

Islamabad, Pakistan

(2024)

Targeted Delivery of Letrozole-loaded Mg-doped Cobalt Ferrite Nanoparticles for Breast Cancer Treatment

By

Huma Ijaz

(Registration No: 00000402052)

A thesis submitted to the National University of Sciences and Technology, Islamabad,

in partial fulfillment of the requirements for the degree of

Master of Science in
Materials and Surface Engineering

Supervisor: Dr. Muhammad Shoaib Butt

School of Chemical and Materials Engineering

National University of Sciences & Technology (NUST)

Islamabad, Pakistan

(2024)

THESIS ACCEPTANCE CERTIFICATE

Certified that final copy of MS thesis written by Ms **Huma Ijaz** (Registration No 00000402052), of School of Chemical & Materials Engineering (SCME) has been vetted by undersigned, found complete in all respects as per NUST Statues/Regulations, is free of plagiarism, errors, and mistakes and is accepted as partial fulfillment for award of MS degree. It is further certified that necessary amendments as pointed out by GEC members of the scholar have also been incorporated in the said thesis.

Signature: _____

Name of Supervisor: **Dr M. Shoaib Butt**

Date: _____18 - 09 - 2024_____

Signature (HOD): _____

Date: _____19/9/24_____

Signature (Dean/Principal): _____

Date: _____19/9/24_____

TH - 1

MSE. 12 - 2022

National University of Sciences & Technology (NUST)

MASTER'S THESIS WORK

Formulation of Guidance and Examination Committee (GEC)

Name: Huma Ijaz   NUST Reg No: 00000402052

Department: Department of Materials Engineering   Specialization: Master of Science in Materials & Surface Engineering

Credit Hour Completed: (21.0) 24   CGPA: (3.64) 3.63

Course Work Completed

S/No:	Code:	Title:	Core/Elective:	CH:	Grade:
1.	MSE-821	Mechanical Behaviour Of Materials	Compulsory	3.0	B+
2.	MSE-811	Materials Thermodynamics	Compulsory	3.0	B+
3.	MSE-881	Manufacturing Processes	Elective	3.0	A
4.	RM-898	Research Methodology	Additional	2.0	Q
5.	MSE-851	Surface Engineering & Characterisation	Compulsory	3.0	B+
6.	MSE-812	Phase Transformation & Microstructures	Compulsory	3.0	B+
7.	MSE-861	Engineering Ceramics And Glasses	Elective	3.0	A
8.	MSE-854	Characterization Of Materials	Elective	3.0	B+
9.	MSE-852	Adv Surface coatings	Elective	3	B+

Student's Signature

Date 04 - Sep - 2023

Thesis Committee

Name: Muhammad Shoaib Butt (Supervisor)   Signature

Department: Department of Materials Engineering

Name: Rumeza Hanif (Cosupervisor)   Signature

Department: Department of Healthcare Biotechnology

Name: Sofia Javed (Internal)   Signature

Department: Department of Materials Engineering

Name: Iftikhar Hussain Gul (Internal)   Signature

Department: Department of Materials Engineering

Date: 04 - Sep - 2023   Signature of Head of Department:

APPROVAL

Signature of Dean/Principal:

Date: 04 - Sep - 2023

School of Chemical & Materials Engineering (SCME) (SCME) H-12 Campus,

TH – 4

National University of Sciences &Technology (NUST)

FORM TH-4

MASTER'S THESIS WORK

We hereby recommend that the dissertation prepared under our supervision by
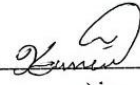Regn No & Name: <u>00000402052 Huma Ijaz</u>

Title: <u>Targeted Delivery of Letrozole-loaded Mg-doped Cobalt Ferrite Nanoparticles for Breast Cancer Treatment.</u>

Presented on: <u>18 Jul 2024</u>   at: <u>1430 hrs in SCME (Seminar Hall)</u>

Be accepted in partial fulfillment of the requirements for the award of Masters of Science degree in **Materials & Surface Engineering.**

Guidance & Examination Committee Members

Name: <u>Dr Iftikhar Hussain Gul</u>   Signature: _____

Name: <u>Dr Sofia Javed</u>   Signature: _____

Name: <u>Dr Rumeza Hanif</u> (Co-Supervisor -ASAB)   Signature: _____

Supervisor's Name: <u>Dr Muhammad Shoaib Butt</u>   Signature: _____

Dated: <u>29th July, 2024</u>

Head of Department
Date 29/7/24

Dean/Principal
Date 30/7/24

School of Chemical &Materials Engineering (SCME)

AUTHOR'S DECLARATION

I <u>Huma Ijaz</u> hereby state that my MS thesis titled "<u>Targeted Delivery of Letrozole-loaded Mg-doped Cobalt Ferrite Nanoparticles for Breast Cancer Treatment</u>" is my own work and has not been submitted previously by me for taking any degree from National University of Sciences and Technology, Islamabad or anywhere else in the country/ world.

At any time if my statement is found to be incorrect even after I graduate, the university has the right to withdraw my MS degree.

Name of Student: <u>Huma Ijaz</u>

Date: <u>30 September 2024</u>

PLAGIARISM UNDERTAKING

I solemnly declare that research work presented in the thesis titled "Targeted Delivery of Letrozole-loaded Mg-doped Cobalt Ferrite Nanoparticles for Breast Cancer Treatment" is solely my research work with no significant contribution from any other person. Small contribution/ help wherever taken has been duly acknowledged and that complete thesis has been written by me.

I understand the zero-tolerance policy of the HEC and National University of Sciences and Technology (NUST), Islamabad towards plagiarism. Therefore, I as an author of the above titled thesis declare that no portion of my thesis has been plagiarized and any material used as reference is properly referred/cited.

I undertake that if I am found guilty of any formal plagiarism in the above titled thesis even after award of MS degree, the University reserves the rights to withdraw/revoke my MS degree and that HEC and NUST, Islamabad has the right to publish my name on the HEC/University website on which names of students are placed who submitted plagiarized thesis.

Student Signature: _____

Name: Huma Ijaz

DEDICATION

" I would like to dedicate this dissertation to my beloved parents and brother for their continuous help and support."

ACKNOWLEDGEMENTS

TABLE OF CONTENTS

LIST OF TABLES

LIST OF FIGURES

LIST OF SYMBOLS, ABBREVIATIONS AND ACRONYMS

Cobalt Ferrite Nanoparticles	CFNPs
Nanoparticles	NPs
Magnesium-Doped Cobalt Ferrite nanoparticles	Mg-doped CFNPs
Nanomaterials	NM

ABSTRACT

Breast cancer is the most common cancer in women globally. Letrozole is an aromatase inhibitor used as an anticancer drug. Conventional Letrozole therapies for breast cancer often cause adverse effects when administered orally or parenterally. Efforts have been made to develop an advanced drug delivery system for breast cancer treatment, aiming to improve drug release accuracy and therapeutic efficacy while minimizing side effects. This study focuses on magnesium-doped cobalt ferrite nanoparticles (Mg-doped CFNPs) as potential drug delivery carrier for breast cancer treatment. Mg-doped CFNPs with the chemical formula $Co_{1-x}Mg_xFe_2O_4$ (where x=0.0, 0.05, 0.10, 0.15, 0.20 and 0.25) were synthesized with different concentrations of 5%, 10%, 15%, 20%, and 25% by the sol gel method with a fine size of 30-70 nm and their characteristics such as surface morphology, structural properties, chemical composition, and charge were investigated using scanning electron microscopy, X-ray diffraction, Fourier transform infrared spectroscopy, and zeta potential analysis respectively. After synthesis, the Mg-doped CFNPs were coated with PEG and encapsulated with Letrozole, which exhibited <10% hemolytic activity across all concentrations, as well as minimal cytotoxic effects on non-cancerous cells (HEK- 293) but exhibited significant toxicity towards breast cancer cell lines (MCF-7, MDA- MB-231).The best results were obtained at a concentration of 25% in both the hemolytic assay and the MTT assay, which indicated that increasing the amount of magnesium in cobalt decreased the toxicity and increased the drug release efficiency of nanoparticles.

Keywords: Magnesium-doped cobalt ferrite nanoparticles, Cobalt ferrite nanoparticles, Breast cancer.

CHAPTER 1: INTRODUCTION

Cancer is being cured and cancer patients are living longer because of early detection and advanced treatments. In an effort to help prevent cancer in people, medical researchers are also discovering independent risk factors associated with the disease. The number of patients suffering from cancer is increasing day by day and is the second leading cause of death. In 2008, the number of deaths from the malignant disease reached 8 million, and by 2030 this number is estimated to reach 11 million [1]. In 2012, 1,671,149 new breast cancer cases were detected worldwide and the number of deaths due to breast cancer was estimated at 521,907 [2]. The four most prevalent kinds of cancer are prostate, colorectal, lung, and breast cancers [3].

Breast cancer is more prevalent among the Pakistani population compared to Western populations. Approximately one in nine Pakistani women are affected by breast cancer, and the country has one of the highest morbidity rates for the disease in Asia. [4]. Traditional cancer treatment methods, such as chemotherapy, surgery, and radiotherapy, have been associated with severe side effects, such as collective radiation doses, high recurrence rates, complications, and low patient satisfaction. In addition, these treatments often do not specifically target cancer cells. [5]. In the latter part of the 20th century, surgeons utilized surgery in combination with chemotherapy and radiotherapy to develop innovative cancer treatment techniques. Currently, researchers are exploring new strategies to reduce the negative effects of chemotherapy, such as using novel drug combinations and targeted drug delivery methods. [6]. Chemotherapy and radiotherapy are often associated with acute side effects, such as bone marrow suppression, skin disorders, hair loss, and fatigue. In addition, these treatments can increase the risk of cancer recurrence. While chemotherapy is effective in killing rapidly growing cancer cells, it also kills or slows the growth of healthy cells. [7].

Nanotechnology offers opportunities to develop new materials and devices with unique properties. In the modern era nanoparticles are used for targeted drug delivery. Nanoparticles with the ideal size and surface properties have been created to extend the

bio distribution of cancer medications by increasing their stay in circulation within the bloodstream [8]. Additionally, they are able to deliver their active drugs to cancer cells by specifically exploiting the particular pathology of tumors. Magnetic nanoparticles have been the subject of intense investigation as the next generation of targeted medication delivery for almost thirty years. Targeted drug delivery and targeted therapy are crucial because they allow a medication to be sent directly to the source of a disease under a variety of circumstances, treating it purposefully and with no negative side effects on the body [9]. Spinel ferrites (MFe_2O_4 such as Cu, mg, Zn, Ni, Co) have been studied in recent years due to their interesting optical, electrical, and magnetic properties. Spinel ferrite nanoparticles (such as Fe, Zn, Cu, Co, Mg) have small size and large surface area, so superparamagnetic behavior has been found to have many applications, including targeted drug delivery [10]. Metal oxide nanoparticles attract attention due to their unique magnetic and other properties such as good chemical stability and good biocompatibility. Individual nanoparticles such as Cobalt ferrite and Magnesium ferrite nanoparticles offer potential applications for cancer treatment [11]. Cobalt ferrite nanoparticles were proposed as a promising solution in biomedical applications, such as magnetic thermo-drug delivery and hyperthermia, biosensors and magnetic resonance imaging. Like all spinel Ferrite, $CoFe_2O_4$, allows for the incorporation of various other metal ions such as magnesium, manganese and zinc to that lattice to create new and interesting materials. This may play an important role in improving physical and magnetic properties [12]. Various methods can be used to synthesize ferrite nanoparticles such as co-precipitation, Sol-gel and ball milling. The sol-gel process (including a heat treatment operation) is likely the most practical and efficient way to create high purity, homogeneous, and crystalline nanoparticles.

Polyethylene glycol (PEG) is hydrophilic polymer. PEG has been established as an excellent stabilizer for NPs. This polymer has been reported to provide improved hydrophilicity and solubility of NPs and helps in improving their biocompatibility and biodegradability [13]. Letrozole is used as an effective drug in the treatment of breast cancer and is highly effective due to its estrogen receptors [14]. Letrozole is an aromatase inhibitor that blocks estrogen synthesis by inhibiting the final step of the estrogen biosynthesis pathway [15].

The aim of this study was to synthesize Magnesium-doped cobalt ferrite nanoparticles (Mg-doped CFNPs) with different concentrations using sol-gel method and use these nanoparticles for safe and targeted drug delivery. Aside from that, effects of magnesium doping and polymer coatings on structural, morphological, and magnetic properties of $CoFe_2O_4$ were evaluated using different characterization techniques (XRD, SEM, FTIR, and Zeta Potential) and *in vitro* drug release, hemolysis and cytotoxicity studies were carried out. Cytotoxicity study was carried out using MTT [3-(4,5-Dimethylthiazol-2-yl)-2,5-Diphenyltetrazolium Bromide] assay. to evaluate the effect of doping and polymer coating on viability of MCF-7, MDA-MB 231 Cancer cell lines in comparison to Hek-293 normal kidney cell lines.

1.1 Introduction to magnetism

An atom is the fundamental building block of everything that exists in this universe. Electrons, protons, and neutrons are the fundamental building block of an atom. Electronic particles move in orbits around the nucleus and also spin around their own axis of rotation. In addition to generating small amounts of currents, electrons also generate extremely small amounts of magnetic field as a result of changing current. Because electrons are a moving charge, the magnetic moment of any existing magnetic field is always aligned with the axis of the rotating charge. The spin motion of the electron is responsible for the generation of the other magnetic moment. It can only move in one of two directions: up or down. The total magnetic moment is always 0 for shells that are entirely filled with material. However, it always has some value in the case of an empty shell.

1.2 Classification off magnetic materials

Depending on their magnetic properties, different materials can be divided into distinct kinds. The most well-known types of magnetism are:

- Diamagnetism

- Anti-ferromagnetism

- Ferromagnetism

- Para magnetism

As shown in figure 1.1. The majority of elements in the periodic table exhibit diamagnetic behavior, but metals in groups I and II, as well as some transition metals, exhibit paramagnetic behavior. Metals that exhibit magnetic behavior in their basic form are categorized as ferromagnetic materials. Examples of ferromagnetic materials are iron, cobalt, and nickel.

Table 1.1: Room temperature magnetic behavior representation of each periodic table elements [3].

The ferrimagnetic behavior of elements cannot be observed in any pure elements; rather, this behavior can only be observed in complexes such as combined metal oxides, for example ferrites, etc.

1.2.1 Diamagnetism

In the absence of an external magnetic field, diamagnetic substances do not produce any magnetic effect. However, anytime an electric field (H) is applied, the motion of spinning electrons begins aligning in the opposite direction of the applied electric field, and the net magnetic moment of the whole system becomes zero as a result of this alignment. The diamagnetic effect is present in all materials to some degree; however, in the vast majority of cases, it is quite feeble and is obscured by the greater value of the paramagnetic behavior or the ferromagnetic term. The susceptibility value is temperature dependent for all diamagnetic materials, and it is not affected by any changes in temperature.
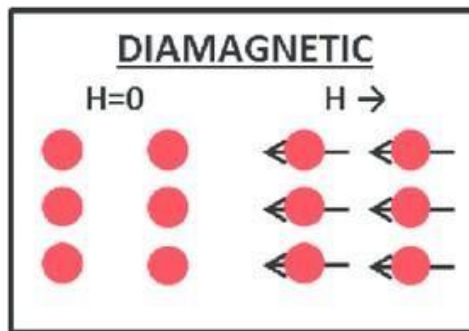
Figure 1.1: Atomic dipole ordering for diamagnetic materials. [4]

1.2.2 Para magnetism

Numerous hypotheses have been proposed to explain the phenomenon of Para magnetism; however, these hypotheses vary depending on the kind of material being considered and can only be true for that particular type of material. The Langevin Model is the basis for one of the hypotheses that have been proposed. This model proposes that every atom has its own magnetic moment, but that owing to the effects of thermal agitation, the orientation of each magnetic moment is completely unpredictable. On the other hand, a field that is applied from the outside might cause a shift in the orientation of the magnetic moments that it produces. It is referred to as paramagnetic behavior when the shift in these alignments occurs in the same direction as the magnetic field that is being applied. Alterations in temperature may have a significant impact on the orientation of

magnetic moments. Because of the rise in thermal agitation, it becomes more difficult for the magnetic moments to align themselves in the same direction as the magnetic field that is being applied as the temperature rises. This is another factor that contributes to a decreased sensitivity.

This property of materials that exhibit paramagnetic activity is frequently referred to as Curie's Law. This is shown in the diagram.

$$x = C/T \qquad\qquad (1.1)$$

Where C is often referred to as the material constant (curie constant). It is a quantity that is depending on the substance being used and varies from one material to another.
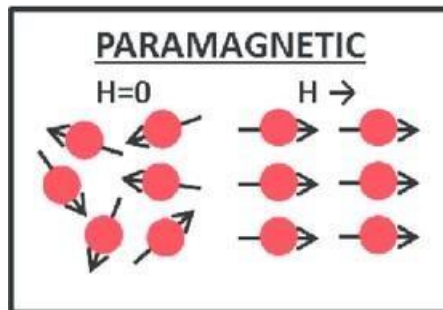
Figure 1.2: Atomic dipole ordering for paramagnetic materials. [4]

1.2.3 Ferromagnetism

Ferromagnetism is a phenomenon that may be described, from the perspective of classical theory, as the existence of a field inside a material. This field makes it possible for the magnetic moments of atoms to interact with one another and align themselves in a parallel fashion. There is no need for an external field to achieve that alignment; nevertheless, the material's internal field is sufficient to magnetise it to saturation. Only iron, cobalt, and nickel exhibit ferromagnetic activity at room temperature and higher when they are present in their elemental forms. When the temperature of a material is raised high enough, the alignment of its atomic magnetic moments tends to shift out of

alignment, turning the material into a paramagnetic state. The name "Curie temperature" was given to this transitional temperature.

1.2.4 Anti-Ferromagnetism

Both ferromagnetism and anti-ferromagnetism refer to the same physical phenomenon. However, what makes this situation unique is that the interaction of magnetic moments results in an anti-parallel alignment of those moments. Because the effects of one magnetic moment are cancelled out by the others, the material behaves as though it were diamagnetic. Only chromium demonstrates this sort of action at ambient temperature, making it unique among all materials. Additionally, this behaviour is sensitive to temperature changes. When the temperature is raised, the increase in thermal motions causes the material to transform into a paramagnetic substance that is located above the transition point. The term "Neel temperature" has come to be used to refer to this particular temperature.
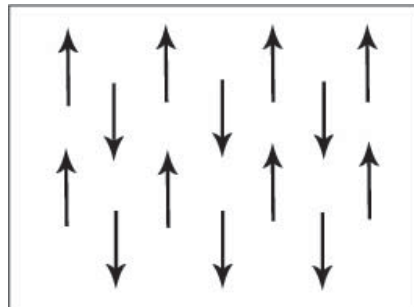
Figure 1.3: Ordering of dipoles for anti-ferromagnetism. [5]

1.2.5 Ferrimagnetism

Ferrimagnetism is a phenomenon that can only be detected in more complex materials, and not in elements like oxides of metals or other simple compounds. There are both parallel and anti-parallel alignments are present in materials that exhibit ferrimagnetism. There is a parallel alignment of magnetic moments in certain sections (domains) of the crystal, but there is an anti-parallel alignment in other regions (domains) of the crystal. The net effect is one that may be described as ferrimagnetic. This property

is identical to that of ferromagnetism, but it can only be shown by substances whose crystal structures are very complicated.

1.3   An overview of ferrites

The word "ferrite" refers to any magnetic oxide in which iron oxide plays a significant role in the crystal structure. This is because ferrite is an all-encompassing phrase. The first magnetic material to ever be identified was a substance called magnetite, commonly known as iron oxide or Fe3O4, which ancient people referred to as a load stone. Other magnetic materials are found much later, with ferrites being the most well-known of these latter discoveries. In their natural state, they are ferrimagnetic cubic spinels, and they combine the characteristics of magnetic materials and electrical insulators in their makeup. The fact that certain characteristics of materials change in a fascinating way below a threshold size is common knowledge. Because of this, research into nano ferrites is necessary for the development of novel applications for these materials in technology.

1.3.1   Historical background of ferrites

The naturally occurring ferrites Fe3O4 piqued man's interest in science and led to its development. The people who lived in the area about 600 B.C. thought that load stone, which is now known to be magnetite, contains an innate life power that is responsible for the attraction that can be seen between magnetite and iron. Du-Bois is credited with conducting the very first investigation on the magnetism of magnetite (1890). Hilpert (1909), on the other hand, was the first person to make ferrites that had a general formula (MOFe2O3). [6]. This this formula M= divalent metal ion an O representing the oxygen atoms.

By conducting the very first ever X-ray examination of magnetic particles, Barth and Posnjak were able to find the inverted spinel structure. This structure is necessary for the presence of ferromagnetic characteristics in ferrites, which were previously unknown. In 1930, Holland became the focus of substantial study in the area of ferrites, and it was at this time that it was proved for the first time how important precise oxygen content is for the quality of ferrite to be 8agnetiz at high frequency. [7]. Verwey found that the

8

electrical conductivity of ferrites, which largely reflects the hopping of electrons between $Fe+2$ and $Fe+3$ ions, may be explained by this phenomenon. It was discovered that ferrite with an inverted spinel structure has ferrimagnetic properties, in contrast to ferrite with a normal spinel structure, which exhibited nonmagnetic properties. Neel first presented his explanation hypothesis on the formation of magnetism in ferrites in the year 1948. In the following year, 1952, he amended his idea. [8]. Through the process of measuring the magnetization of the mixed ferrites, Gorter and Gaillard were able to demonstrate the experimental verification of Neel's hypothesis. By conducting neutron diffraction investigations, Shull and Strauser were able to demonstrate that the Neel's hypothesis is correct for both magnetite and zinc ferrite. Koop's research on ferrites revealed that they had a high conductivity, and he coupled this property with a high dielect'Ic constant to arrive at the formula. [9].

1.3.2   Soft ferrites

Soft ferrites are defined as those that are capable of being 9agnetized and demagnetized with relative ease by the application and removal of an applied field. They are only able to maintain their magnetic state when they are subjected to the effect of a magnetic field. Both the hysteresis loop and the coercivity values of soft ferrites are significantly reduced. This indicates that the magnetization of the material may readily change direction without suffering a significant loss of energy. [10]. An ideal ferrite have properties:

- Low coercivity

- High saturation magnetization

- Zero remanence

- Zero hysteresis loss

- High permeability [11].

1.3.3   Hard ferrites

They are also known as **Ceramic Magnets**. Because of their high coercivity, hard ferrites are extremely difficult to demagnetize. Magnets for refrigerators, loudspeakers, and electric motors for tiny appliances are all examples of products that benefit from the employment of these permanent magnets. Because soft ferrites have a low coercivity, they can alter their magnetization quickly and function as magnetic field conductors.

1.4   Ferrites: their constituent parts

Ferrites has general chemical formula $M^{+2} Fe2+3 O4-2$ where M= divalent metal ion. Some examples given in ionic form:

- Nickel (Ni^{2+})

- Zinc (Zn^{2+})

- Magnesium (Mg^{2+})

- Cobalt (Co^{2+})

- Copper (Cu^{2+})

- Iron(Fe^{2+})

1.5   Structure of ferrites

W. H. Bragg and Nishikawa discovered spinel ferrite in 1915. [12]. Ferrites' crystal structure is like spinel's (MgAl2O4). Spinel ferrite's structure is simplest. It has 32 oxygen ions per unit cell. Anions in FCC lattice are packed between two interstices. In figure 1.5(a) where, **solid lines** and the **dotted lines** represent the top and bottom layers of oxygen spheres respectively. To form a spinel structure the ionic radius of divalent metal ion M must be less than or about 1 Å. And most of the divalent metal ions (listed above) that form spinel structure have their ionic radius between 0.6 to 1Å [13]. If the ionic radius of M is greater than 1 Åthen the electrostatic Coulomb force required for the stability of crystal are insufficient. For examples Ca^{+2} (ionic radius 1.06 Å) does not form spinel crystal, where in Mn^{+2} 0.91 Å) does form spinel crystal. In figure 1.5, there are two kinds of interstices are present, denoted by letter (A) (tetrahedral site) and (B) (octahedral site).
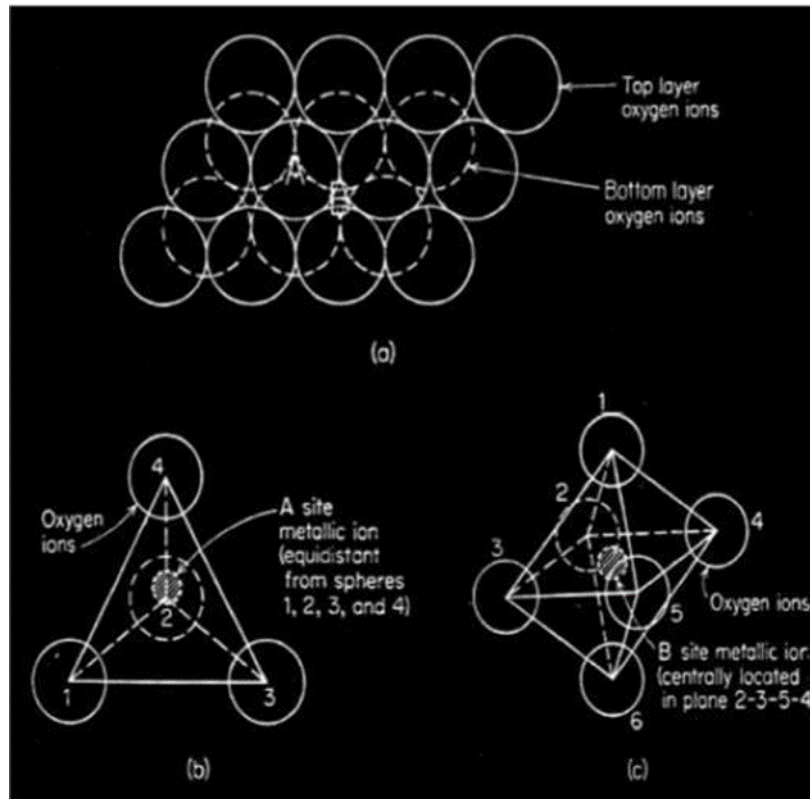
Figure 1.4: Ionic positions (a) Hexagonal Close packing (b) Tetrahedral (A) site (c) Octahedral (B) site (An et al. 2022).

There is total 96 interstices are in spinel structure, 24 filled by a cation and total of 72 remains empty. The sites occupied by cations are classified as either tetrahedral (A)or octahedral or (B) sites. The (A) site only contain eight interstices are which are occupied and on A site each one is surrounded by 4 oxygen atom and on the (B)site, sixteen are occupied and each one is surrounded by six oxygen ions [14] as shown in figure 1.5.

1.6   Classification of ferrites

It is possible to categorize the ferrite according to the type of crystal structure it possesses. They come in three distinct configurations: hexagonal, garnet, and spinel. Magnetic garnets and other applications that require permanent magnetism rely heavily on hexagonal ferrites. The use of garnets in microwave technology is particularly unique, and spinel ferrites play an important role in a wide variety of applications in the electrical, electronic, automotive, and computer industries.

11

1.6.1 Garnet

Garnets have chemical formula of M3(Fe5O12), crystal where M can be (yttrium (Y), rare-earth) ion for example.

- Gadolinium   Erbium

- Terbium   Thulium

- Dysprosium   Lutetium

- Holmium   Europium

The structure of garnet ferrites is identical to that of the silicate mineral garnet, and their chemical formula is M3(Fe5O12), where M can either be the element yttrium or one of the rare earth ions. Garnets have dodecahedrasites in addition to tetrahedral and octahedral sites, like those found in spinels; however, spinels only have tetrahedral sites. Therefore, the net ferrimagnetism is a complicated result of the antiparallel spin alignment that occurs between the three different types of sites. Garnets have a high magnetic hardness as well.

1.6.2 Hexagonal ferrite

The chemical formula for so-called hexagonal ferrites is M(Fe12O19), where M is typically one of the elements bariums (Ba), strontium (Sr), or lead (Pb). The structure of the crystal is quite complicated, but it can be simplified by saying that it is hexagonal and has a distinct c axis, also known as a vertical axis. In the fundamental structure, this is the axis that facilitates magnetization most easily. Hexagonal ferrites are considered "hard" due to the fact that the magnetization cannot be easily reoriented along another axis. Three metal ions occupy hexagonal lattice sites.

- Tetrahedral site

- Octahedral site

- Trigonal-bi-pyramid

Six (6) oxygen ions surround each metal ion. Hexagonal ferrites have a complicated crystal and magnetic structure.

1.6.3 Spinel ferrite

Spinel ferrites are soft ferrites means they can easily change their direction of magnetization by applying external field. They have cubic in structure. In spinel ferrites the distribution of metal ions (divalent/trivalent) at both octahedral and tetrahedral sites can greatly influence their properties. Barth and Ponjak observed the different arrangement of cations in spinel ferrites. And on the basis of different cationic distribution, they can be categorized differently as [15].

- Normal spinel

- Inverse spinel and

- Random spinel ferrite
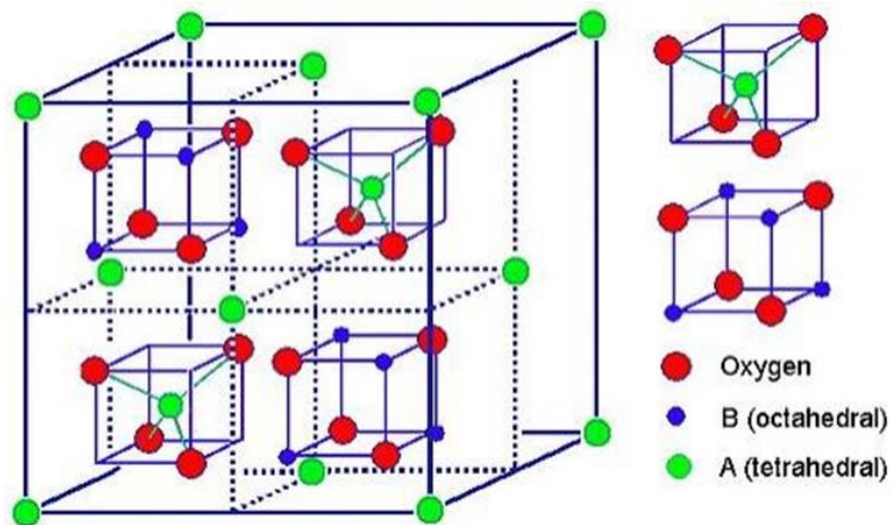
Figure 1.5: Unit cell of spinal ferrites showing tetrahedral and octahedral sites [16(Joseph and Pamu 2015)6]

1.6.4   Spinel ferrites

In typical spinel ferrites, divalent metal ions occupy (A) sites while trivalent metal ions occupy (B) sites. Because the (A) site in these spinel ferrite crystals does not have any magnetic ions, there are no A-B interactions between the crystals. They only have B-B interactions, in which half of the magnetic ions align in one direction and the other half align in the opposite way, leading to nonmagnetic ferrites. In a spinel crystal, each unit cell is composed of eight FCC cells. Anions, which are typically oxide ions (O^{-2}), are the ones that occupy the FCC lattice sites. The trivalent BIII cations fill one half (1/2) of the octahedral spaces, whereas the divalent AII cations fill just $1/8^{th}$ of the vacancies in the tetrahedral structure. Normal spinel ferrites may be represented by ZnFe2O4 and CdFe2O4, for instance. The formula for the cationic distribution of typical spinel ferrite is as follows:

$$(M^{+2})A\ (Fe^{+3})\ B\ O_4{}^{2-}$$
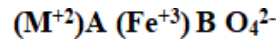
Where, M=divalent (metal) ion.

1.6.5   Inverse spinel ferrites

There are 1/8th- and 1/4thof-an-octahedral BIII ions, with AII taking up 1/4 of the void space, while the other half of BIII ions fill up the remaining spaces in the octahedron. There are many ways to express it, such as: (BIII)tet(AIIBIII)octO4 Fe+3 is located at the tetrahedral site (A) of the inverse spinel ferrites, while the other remaining trivalent ions (Fe+3) and the all divalent metallic ions (M+2) are located in the (B) site. MnFe2O4, CoFe2O4, and NiFe2O4 are common inverse spinel ferrites. They are the most basic ferrites.The cationic distribution for inverse spinel ferrite is given by

$$(Fe^{+3})A\ (M^{+2}\ Fe^{+3})B\ O_4{}^{-2}$$
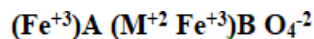
1.7   The cation distribution

The distribution of cations in spinel ferrites has a significant impact on the electrical and magnetic characteristics of the material. The distribution of iron and M^+ the octahedral and tetrahedral positions of the spinel lattice is determined by a wide variety

of variables. Several different approaches might be used to ascertain the cationic distribution. Certain ones of them are:

- X-ray diffraction methods [17]

- Neutron diffraction method

- Mossbauer spectroscopy [18]

- Magnetic susceptibility measurement

- Infrared absorption spectroscopy [19]

Calculations of the X-ray intensity ratio are performed during the X-ray diffraction method for the planes (220), (311), (400), and (440), among others. Theoretical and experimental values of the X-ray intensity ratio are compared at this point in the process. It is generally accepted that the correct cationic distribution is the combination for which theoretical and experimental values for cations appear to be relatively close to one another.

1.8   Factors effecting cationic distribution

Some of the factors are listed below which can influence the cationic distribution at tetrahedral and octahedral sites.

- Ionic radius

- Electronic configuration (Distribution of electrons)

- Synthesis Method

1.8.1   Ionic radius

Since the octahedral (B) site in the spinel lattice has a larger ionic radius than the tetrahedral (A) site, big cations such as Co^{+2} and Ni^{+2} would typically choose to occupy the octahedral (B) sites, and tiny cations will take the (A) tetrahedral sites..

1.8.2 The electronic configuration

It is a common observation that ions with filled d-shell often have tendency to form sp^3 hybrid orbital and occupy the tetrahedral(A)sites for example Zn^{+2} and Ge^{+4}, whereas the ions with d^3 and s^8 electronic configuration tend to form $d^3 sp^3$ hybridorbital and occupy the octahedralsites in spinel. For example (C h r o m i u m Cr^{+3} and (Nickle)Ni^{+2} [20].

1.8.3 Method of preparation

It has been found that the technique of preparation may also have an influence on the distribution of cationic at tetrahedral and octahedral sites. The heat treatment of the material, also known as sintering, has a significant impact on the cationic distribution. Different characteristics may be shown by identically composed materials, even if they were created using different processes.

1.9 Applications of ferrites

Spinel ferrites offer a significant amount of promise for use in daily life. Even though a significant amount of study has already been conducted in the subject of ferrites, scientists and technologists continue to have an interest in ferrite materials. Recent study has shown that the doping of ferrites is of particular interest to the researchers. Which may be made using a variety of different compositions, synthesis processes, and with varying concentrations of cationic groups, all of which have a significant impact on the material's characteristics, including its electrical, dielectric, and magnetic qualities. Ferrite materials are among the most significant types of magnetic materials. These materials find use in a variety of applications, including power conditioning, electromagnetic devices, electromagnetic wave absorbers, magnetic inks for bank cards, recording media, and other similar areas. The following is a list of some of the most important areas where ferrites may be used:

- Medical diagnostics and treatments

- Drug delivery Magnetic storage

- Magnetic shielding

- Magnetic sensors

- Electromagnetic interference suppression

- Pollution control

1.9.1 *Objectives of this research*

The objectives of this research work are as follows:

- Preparation of CoFe2O4 single phase spinel nanoparticles using sol gel synthesis.

- Preparation of Mg doped Co(1-x) (Mg)x Fe2O4 nanoparticles.

- Material characterization using XRD, FTIR, SEM and Zeta Potential.

Study the effect of Mg doped cobalt ferrite nanoparticles for biomedical application like drug delivery.

CHAPTER 2: LITERATURE REVIEW

2.1   Synthesis of nanoparticles

Synthesis of nanoparticles can be done by using two major approaches.

1. Top down approach

2. Bottom up approach

The top-down strategy begins with huge structures and uses finer technologies to build smaller and finer structures, such as lithography, ball milling, laser ablation, electro spinning, arc discharge, etc. The bottom-up approach combines atoms, molecules, and clusters to generate nanoparticles... Examples of bottom-up approach are wet chemical synthesis, chemical vapor deposition (CVD), hydrothermal synthesis, physical vapor deposition (PVD), MBE, self-assembly etc.
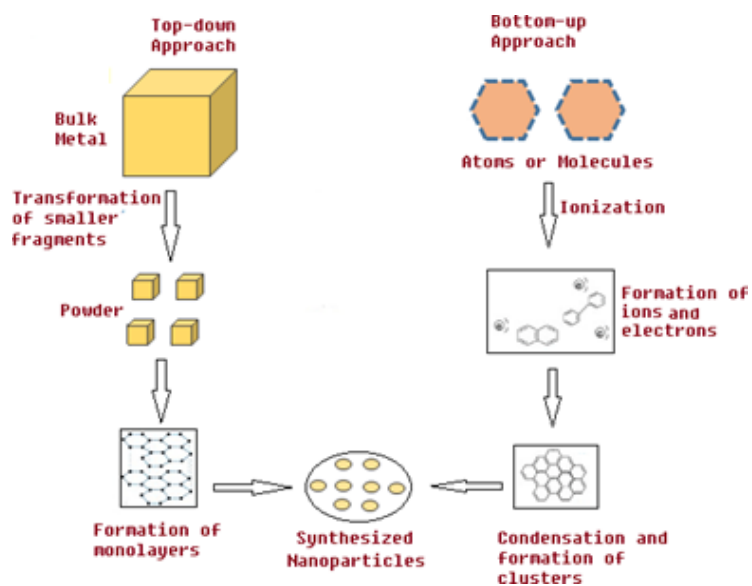
Figure 2.1: Top-down and bottom-up approach

Both techniques have some advantages and disadvantages. In top-down approach it is difficult to attain homogenous nanoparticles and of smaller size and also a significant amount of impurity is always present.

While in the use of bottom-up technique implementation cost is likely to be higher. There are different methods for the synthesis of nanoparticles. Each method has its own advantage and disadvantages. Some of the methods are shown in the following figure.
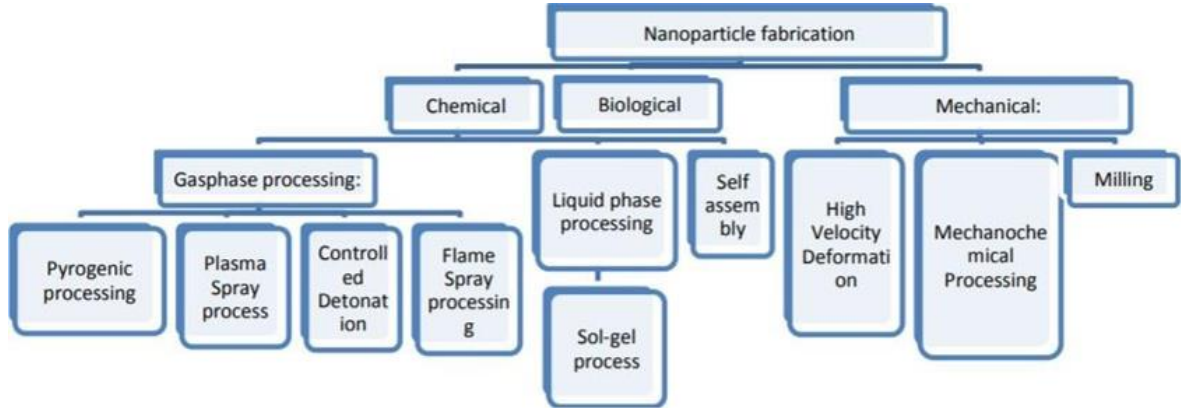
Figure 2.2: Scheme of fabrication of Nanomaterials techniques.

Ferrites nanoparticles synthesis can be carried out using different routes for example hydrothermal[21], solvothermal[22], co precipitation[23], sol gel, micro emulsion and other methods. Synthesized ferrite's properties depend on synthesis route and conditions. A lot of work has been done and is still being done on ferrites for various applications.

2.2   Sol-gel synthesis

2.2.1   Introduction

The sol gel synthesis is kind of inorganic polymerization. It was firstly described by Ebelmann in 1864 [24]. This allows nanomaterials to be made from colloidal solutions. Monoliths, crystallised nano pigments, and thin layers are examples. They are centred on polymerization reactions. Sol-gel, metal alkoxide, and pechini are the three types of this.

The sol-gel method focuses on chemical compound growth in a solution. Following interactions between the species and the liquid, the sol transforms into a three-sided channel that grows in the solvent. After that, the process is frozen, and the sol-gels are deformed solid material by removing liquid from the air-gel or evaporation.

One advantage of the method is the ability to control the size and uniformity of the material spread. They allow for the production of large fibre parts. However, one major drawback of the technique is that the precursors are prohibitively expensive, yielding low weight products that are hazardous to human health.

A sol consists of colloidal suspension, in which solid particles (solute) are dispersed in some liquid medium (solvent). The common precursors mostly used for sol–gel synthesis is

- Inorganic salts (chlorides, nitrates)

- Organic compounds

The sol–gel process hydrolyzes and condenses metal precursors to form a 3D inorganic network. In ferrites, metals or metalloids are surrounded by ligands, such as metal nitrates. Water-soluble nitrate salts. This is hydrolysis. In this reaction, hydroxyl ion attaches to metal ion (M).

$$M(OR)4 + H2O \rightarrow HO - M(OR)3 + ROH$$

On the completion of hydrolysis all OR groups replaced by OH.

$$M(OR)4 + 4H2O \rightarrow M(OH)4 + 4ROH$$
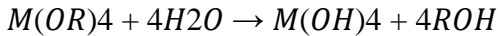
Here could be another scenario, when hydrolysis stops while the metal is partially hydrolyzed M (OR)4-X (OH)X. These two molecules can take part in condensation by linking together. This process liberates water molecule as shown in below reaction.

$$(OR)3M - OH + HO - M(OR)3 \rightarrow (OR)3M - O - M(OR)3 + H2O$$
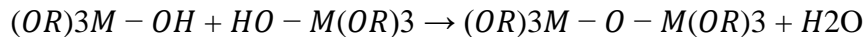
This type of continuous reaction builds large metal containing molecule which is called gel. It contains a continuous solid structure which is amorphous in nature but can be crystallized on heating treatment. For the preparation of ferrites sintering of the prepared samples need to be done at elevated temperatures.

A flow chart of sol-gel method is shown below:
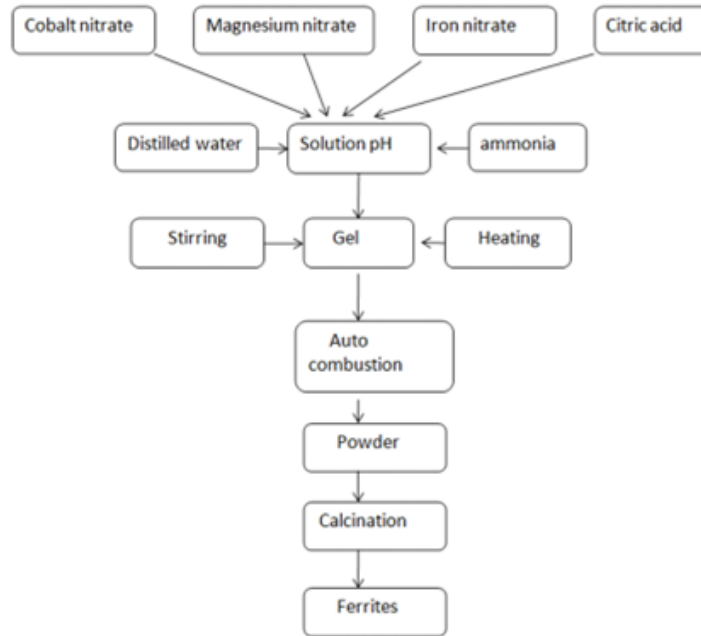
Figure 2.3: Flow- chart of sol-gel combustion method

2.2.2 *Effect of different factors on Sol-gel synthesis*

Many factors can affect the structure, morphology, particle size etc. during the synthesis. Some of them are listed below

- Effect of chelating agent

- Effect of pH

2.2.3 *Effect of chelating agent*

Precursors (metal nitrates) and chelating agents (urea/citric acid [25]/glycine/hexamethylenetetramine) are used to make powder ferrite nanoparticles. Metal nitrates and citric acid are usually mixed 1:3. The ratio and type of chelating agent affect structural, magnetic, cationic, and particle size [26]. Chelating agents burn differently. Hexamethylenetetramine and glycine autocombusted quickly. Citric and tartaric acids took over 30 minutes to burn. Urea auto-combustion took 2-3 minutes [27].

2.2.4   Effect of pH

Ammonia is typically used in sol-gel synthesis because it allows for greater control over the pH value of the solution. It acts as a catalyst for the process of hydrolysis, which is followed by condensation. The pH values have a significant impact on the combustion rate. [28]. The pH values in the range of 7-8 cause a rapid gelation, which is perfect for the production of nanoparticles of minute dimensions. While pH values between 2 and 3 produce little to no gelation and are therefore perfect for constructing an extensive network.

2.3   Literature study

Because ferrites are good dielectric materials, they have a wide range of applications, such as in microwave devices and in the delivery of targeted drugs [29], data storage sensors [30], catalysis [31], core materials and electromagnetic absorbers [32] etc.

Gul et al. prepared Co1-x NixFe2O4 nanoparticles, by co precipitation, while x varying from 0.0 to 0.5. The measured particle size ranged from 14nm to 21nm. The value of off saturation magnetization and coercivity decreased as the nickel concentration increased. It was concluded that the decrease in magnetization was due to an increase in nickel ions at octahedral sites because of the low magnetic moment of nickel ions (2μB). [33].

Pardeep et al. synthesized MgFe2O4 nanoparticles using sol-gel (wet chemical) route. They've done XRD, SEM, and FTIR analysis, and the results show that the samples are single phase and crystalline. It was also found that cation distribution can alter the structure of a substance, as well as its other properties. A decrease in the value of magnetic moment and saturation magnetization was also reported in comparison to bulk ferrite by these scientists. [34].

Smitha et al. prepared magnesium ferrite nanoparticles using the sol gel method. The XRD data and FTIR results confirms single phase of spinel structure formation with no impurity present. The temperature variation of dc conductivity was also studied and reported the Decrease in conductivity occur till temperature 323K because of the water

absorbed in the sample. According to the magnetic studies reveals that the sample shows ferromagnetic behavior at low temperature [35].

Bortnic et al. synthesized CoFe2O4 Sol-gel nanoparticle synthesis is a low-cost and non- toxic method. As a gelation agent, pectin is used, and sucrose is used for poly-condensation. In order to confirm the single phase spinel structure, XRD and FTIR data were collected. The TEM determined the grain size to be between 20 -75 nm. [36].

Thankachan et al. Co-precipitation and sol-gel methods were used to create Magnesium ferrite nanoparticles. A typical sol-gel synthesis crystallite size of 9nm and a co- precipitation crystallite size of 12nm were found using XRD analysis. XRD and FTIR confirmed the single-phase spinel structure in both synthesis methods. Both samples are ferrimagnetic with a hysteresis, according to the magnetic measurements. When compared to the sol-gel sample, the saturation magnetization value for the co-precipitation sample is very low. The low value of the oremanent ratio demonstrates that the sample that was prepared via the co-precipitation route is isotropic. The Maxwell–Wagner theory was used to determine the dielectric constant and loss value as a function of frequency. Temperature-dependent values for dielectric and ac conductivity have been reported. [37].

Moradmard et al. synthesized Ni 1-xMgxFe2O4 by using co precipitation route. . Single phase structure was confirmed by X-ray diffraction analysis, and the overall crystallite size increased when magnesium was added. Also investigated were dielectric properties as well as magnetic properties. Magnesium increases coercivity and decreases magnetization in magnetic measurements. Increase in coercivity is related to the replacement of Fe^{+3} by Mg^{+2} ions at octahedral sites. The dielectric properties like dielectric constant were investigated. Decrease in the dielectric values has been reported. Koop's theory explains the decrease in dielectric loss value with increase in frequency [38].

Mahalakshmi et al. prepared nickel ferrite nanoparticles (Nix Fe3-x O4). They reportedthe decrease in dielectric values and increase in dielectric loss values. The report also shows the dependence of ac conductivity on nickel concentration as it was only

dependent on the conduction of electrons between Fe^{+2}/Fe^{+3} ions but also on Ni^{+2}/Ni^{+3} ions. Conductivity values increased with the increase in frequency [39].

Hashim et al. studied the effect of cr+3 doping in Ni-Mg ferrite nano particles. Prepared materials were analyzed using XRD, FTIR and Scanning electron microscopy. They have confirmed the mixed spinel nature of the material. They have reported that increase in Cr^{+3} content cause decrease in lattice constant values. which was expected because the radii of Cr^{+3} is less than Fe^{+3}. The magnetic analysis shows a decrease in saturation magnetization. Which explains the low exchange at A and B site [40].

Velhal et al. synthesized Co1-x Nix Fe2O4 successfully by using simple sol-gel route. The crystalline structure was confirmed using xrd analysis while little impurity was also observed of phase Fe2O3. They have reported that the increase in nickel content not only improves crystallite size but also improves the value of magnetization. The general trend of dielectric constant and dielectric loss was seen which was decreasing with frequency. Increase in magnetization and decrease in coercivity was observed and their behaviors was temperature dependent. [41]

Velho Pereira et.al To test the antibacterial activity of CoFe2O4 nanoparticles against two multidrug resistant clinical pathogens, the colony forming units (CFU) and bactericidal potencies of pristine and doped CoFe2O4 nanoparticles were measured. Following a 24- hour incubation period, the nanoparticles under study had a bactericidal effect on the tested pathogens. The E. coli bactericidal potency of the pristine CoFe2O4 nanoparticles was 53.33 percent. The bactericidal potency was increased by 83.73 percent when Nd and 62.4 percent when Bi were added as doping agents. [42].

Sanpo et al. It has been demonstrated that nanoparticles of CoFe2O4 have the potential to possess antibacterial properties that are effective against bacterial pathogens, particularly bacillus cereus. On the other hand, we discovered that the inhibitory effect of CoFe2O4 on bacterial growth would be increased if the nanoparticle's concentration increased (from 0.06-0.48 mg/ml). This was another finding that we made. These findings are consistent These findings are consistent with those found in another study[43]

K. Vijaya Kumar et.al synthesized copper substituted nickel ferrites nanoparticles with series of different compositions of copper. Citric acid was used as a fuel for combustion in sol gel synthesis. Crystallite size was measured using XRD data which was in range of 40-60nm. This analysis also confirms the cubic spinel nature of material. [44].

S. Velho-Pereira et al report that systems containing cobalt ferrite nanoparticles have an antibacterial activity against multidrug-resistant clinical pathogens, specifically the Gram- positive bacteria S. epidermidis and the Gram-negative bacteria E. coli. In most of the cases, doping resulted in a significant increase in the bactericidal effect; however, in the case of doping with Gd against E. coli, doping resulted in a reduction in the bactericidal effect in comparison to the unadulterated nanoparticles. As a result, these nanoparticles have the potential to be utilized as a weapon in the fight against and the containment of epidemics of diseases that are potentially fatal. [45]

Y.C yang et al. studied nickel ferrite and its electrical, magnetic and structural properties. Also composite of nickel ferrite with transition metals and rare earth metals was studies. The particles were prepared by different routes including sol-gel method and co precipitation method and a comparison id made between them. The particles prepared by sol-gel method were big in size, highly resistive, ferromagnetic and multi domain. The prepared particles can be used in applications involving high frequency. The particles prepared by co precipitation method were smaller in size, paramagnetic and had single domain. The prepared particles are applicable in magnetic resonance imaging, drug delivery, medical applications etc. when nickel ferrite is doped with rare earth element. The reduction in magnetization is observed. The increase in coercively is observed by adding transition metal. The decrease in dielectric loss is observed when doped with rare earth metal ions. Particle size increase in case of doping with transition elements. The lattice constant is also observed to increase with doping. The unit cell is also observed to expand. Further studies suggested that dielectric and electrical properties, for example dielectric loss of doped nickel ferrite is observed to decrease and resistivity is observed to increase by doping with transition metals [46].

CHAPTER 3: MATERIALS AND METHODS

3.1   Synthesis of Mg-doped Cobalt Ferrite NPs

For the preparation of composition $Co_{1-x}Mg_xFe_2O_4$, where x= (0.0, 0.05, 0.10, 0.15, 0.20 and 0.25) sol gel synthesis technique has been used**.**

3.1.1   Apparatus used

- Beakers

- Magnetic stirrer

- Hot plate

- Permanent magnet

- Spatula

- Mortar and pestle

- Furnace

- Crucibles

- Aluminum foil

- Glass vials

3.1.2   Materials used

- Ammonia [NH_4OH]

- Deionized water

- Citric acid [$C_6H_8O_7$]

- Cobalt nitrate (Hexa-hydrated [Co (NO3)2. (H2O)6])

- Magnesium nitrate (Hexa-hydrated [Mg (NO3)2])

- Iron nitrate (nano-hydrated [Fe (NO3)2.9H2O]).

Sigma Aldrich supplied all of the analytical grade ingredients listed above.
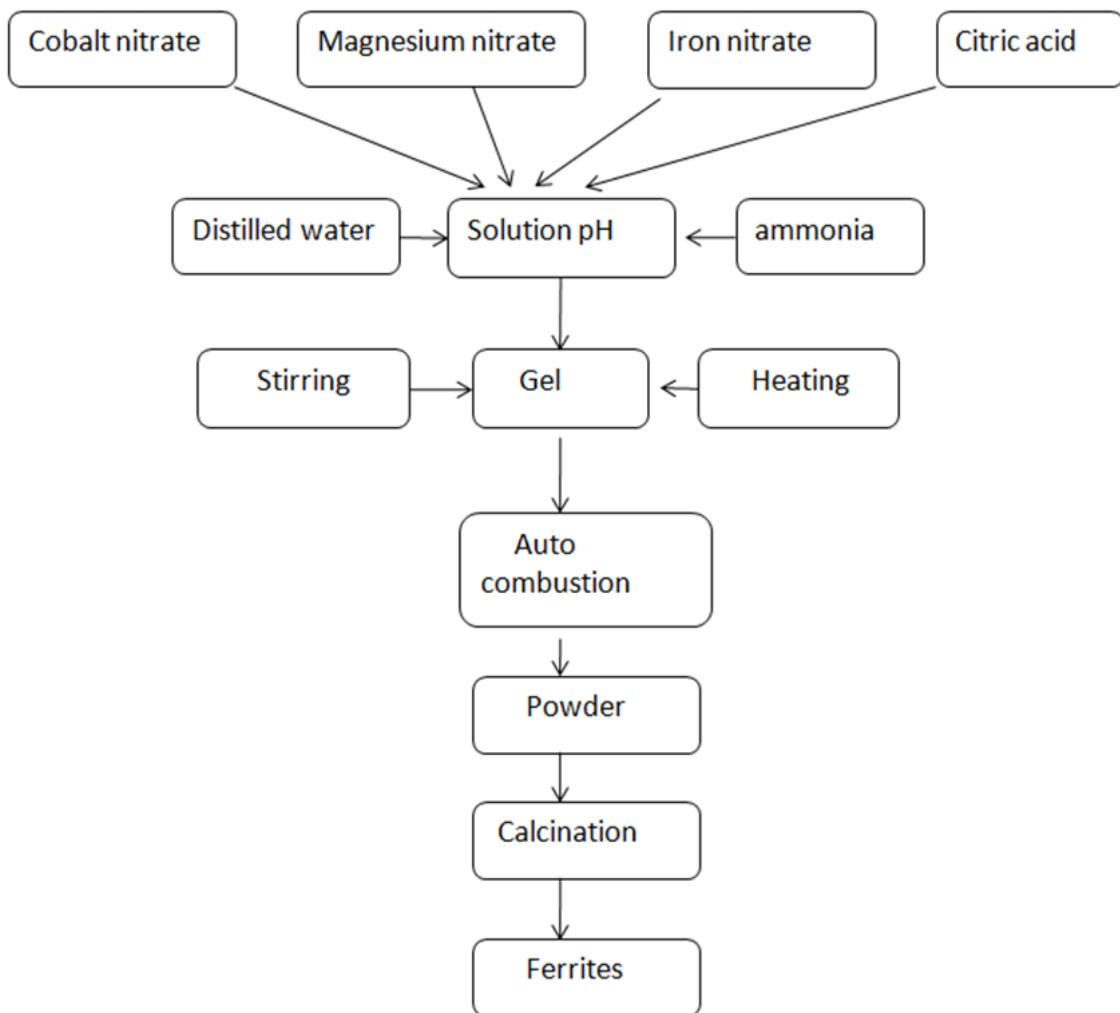
3.1.3   Procedure

Figure 3.1: Flow chart diagram for the synthesis of ferrites samples preparation.

For sol gel synthesis metal nitrates and citric acid ratio was kept as 1:3 and following stoichiometric ratio formula was used to calculate the composition of different chemicals utilized in the process.

The following salts were purchased from Sigma Aldrich: ammonia [NH_4OH], deionized water, citric acid [$C6H8O7$], cobalt nitrate (Hexa-hydrated [Co (NO3)2. (H2O)6]), magnesium nitrate (Hexa-hydrated [Mg (NO3)2]), and iron nitrate (nano-hydrated [Fe (NO3)2.9H2O]).

The remarkable structural, electrical, and magnetic properties of ferrites, a large class of magnetic oxides, make them suitable for a wide range of applications. The choice of synthesis route depends on various factors like to obtain desired structure, cost, and good temperature control [16].

Mg-doped CFNPs with different compositions (0.05,0.1,0.15,0.2,0.25) were prepared by the sol-gel method. The specific amount of iron nitrate (nona-hydrated), cobalt nitrate (hexa-hydrated) and magnesium nitrate(hexa-hydrated) was measured. The molar ratio between nitrates and citric acid were kept 1:2.

The number of specific salts were added to the deionized water separately and then all salts solution was mixed together. The solution was then stirred at 90˚C [17]. After mixing the solution well, ammonia solution was added dropwise to neutralize the pH.

When the pH reached 7, the solution temperature was maintained at 90 °C and the solution was stirred for approximately 4 h to transform into a gel. Each solution contained citric acid as the fuel agent at a molar ratio of 1:2 [18].

The prepared gel was subjected to a self-propagating combustion process at the next stage with an increase in temperature to 300 °C for ~1 h, after which a flaky loose powder was obtained. [19].

To obtain the desired degree of crystallinity, grinding was carried out using a flaky loose powder, after which the powder was calcinated at 8000C in a muffle furnace. The synthesized NPs are shown in Figure 1.
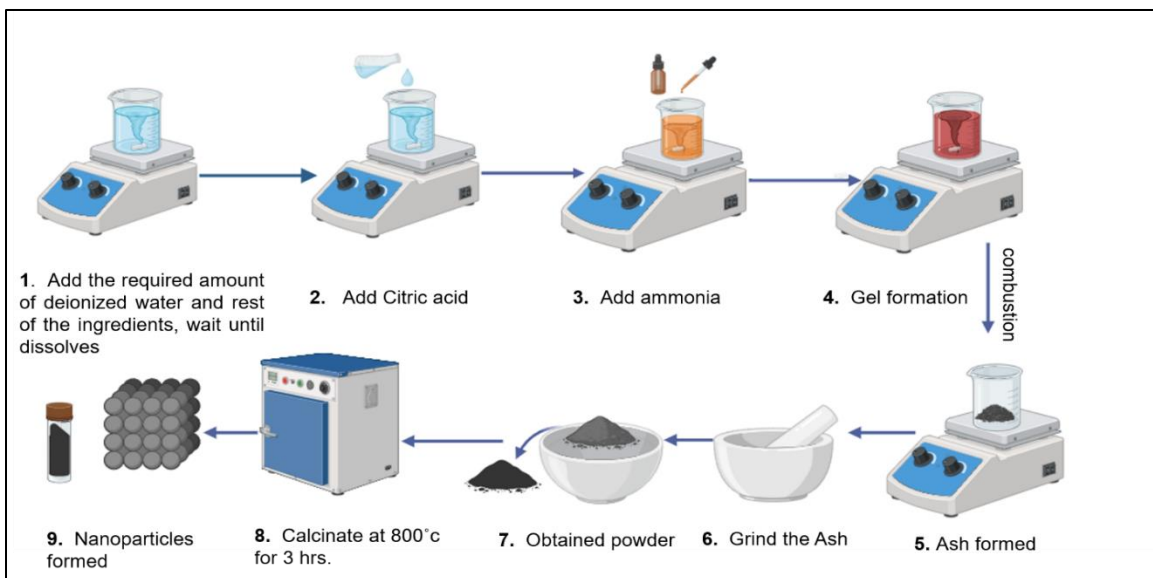
Figure 3.2: Synthesized Mg-doped CFNPs at different concentrations.

CHAPTER 4: CHARACTERIZATION

The properties of synthesized $Co_{(1-x)}(Mg)_x Fe_2O_4$ are analyzed by performing some specific analysis techniques. One of the analysis techniques can be used to obtain information about a material's properties, including its physical and chemical properties, as well as other information about the material, including its morphology, lattice parameter, structure, and so on. A concise introduction to the various methods of character development will be provided in this chapter. The following methods of characterization may be utilized in the process of analyzing the off-synthesized composite.

4.1   X-Ray diffraction technique

It is a vital tool for determining the degree of crystallinity and the structure of a material. Through the utilisation of XRD, one is able to obtain crystal clear information regarding structural strain, crystal defects, average crystallite size, crystallographic orientation, and degree of crystallinity. Powder diffraction, the Laue method, and the rotating crystal method are the three distinct approaches that can be utilised in the process of determining the structure of a crystal. If the powder diffraction method is used, then there are two methods that can be used to determine the size of the crystal.The techniques are as follows.

- Debye Sherrer Method

- Diffractometer method

The sample was in the form of fine grinded powder. Copper, Molybdenum etc. can be used as a target material. Cu (k-Alpha) 1.54060Å source was the XRD source used for analysis in this case.

4.1.1   Basic principle of XRD

The sample has been prepared for examination. A beam of X-rays is directed down onto the sample, where it is then reflected by the crystal's plane. The X-rays that meet the

30

material are reflected by the crystal plane. Interference occurs only in situations in which the incidence angle and the reflection angle are exactly the same. The Bragg"s Law is given by

$$n = 2dSin\theta$$

where n=1,2,3….. Representing order of interference, θ is incidence angle, d is Interplanar distance and λ is wavelength of incident X-ray. The Bragg"s law states that the incident ray is reflected only when the path difference between set of planes is integral multiple of 2dsinθ [47]. The set offplanes are at an equal distance of d.

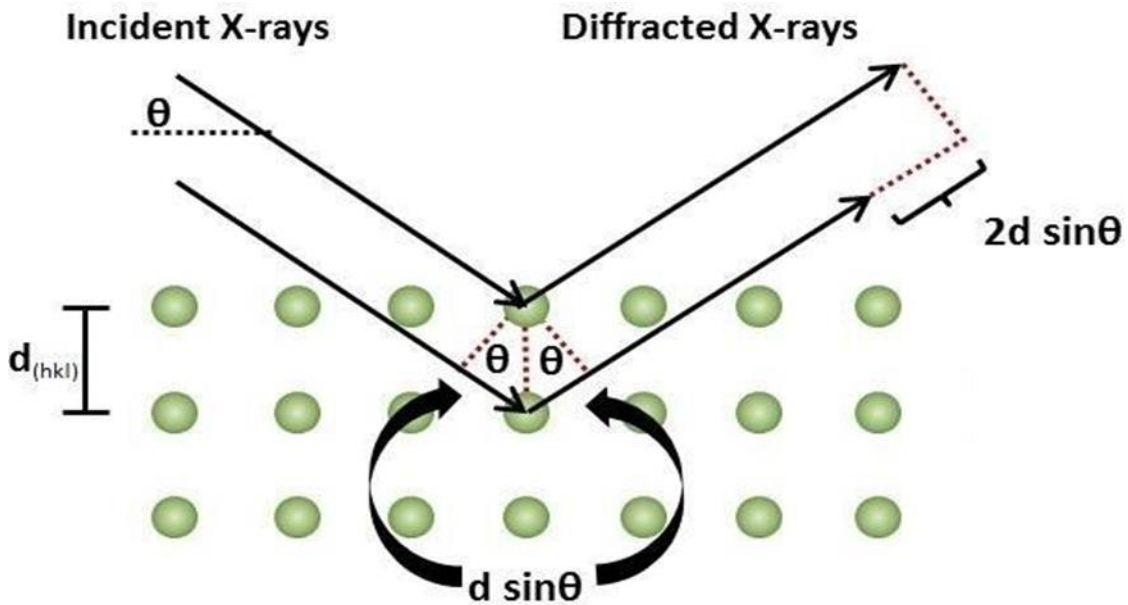**Figure 4.1:** Incident x-ray beam scattered by atomic plane in a crystal [48]

This equation is known as Bragg"s equation. The condition for reflection in above mentioned equation is that it only occur when θ<2d. For this reason, visible light cannot be used. For the characterization of a three-dimensional structure three techniques are usually used which are as follows:

- Laue Method

- Powder method

- Rotating Crystal Method

The XRD analysis will be performed on a sample that has been reduced to the form of nanopowder for examination. Therefore, the powder method is going to be the one that is useful for the sample that is desired. Powder diffraction is the method that should be used when evaluating powdered samples and when there is not an available single crystal of an acceptable size. This is because powder diffraction provides the most accurate results. The procedure for carrying out this experiment involves reducing the sample to a powder through crushing. After that, the sample will be positioned in a rectangular-shaped plate made of either aluminium or glass. After that, a beam of monochromatic X-rays is pointed in the direction of the powdered sample.
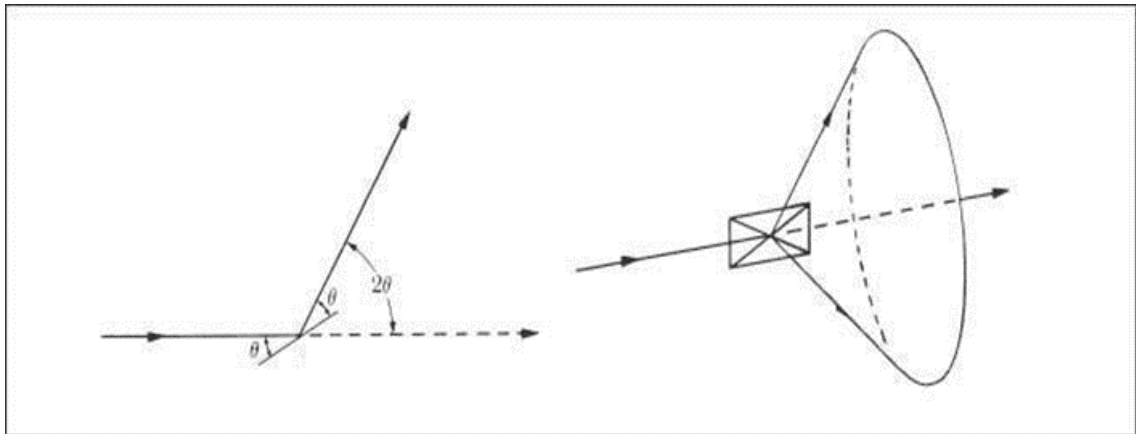
Figure 4.2: Diffracted cones of radiations forming in powder method [48]

Consider the reflection as shown in figure. The portion of the sample that is in the form of powder is oriented in such a way that it will be possible to reflect it because it is present at the appropriate Bragg angles. The path of motion of the reflected beam will be along the surface of the cone when the plane is rotated about the beam which is made incident. In the case of our particles, the reflection does not take place across the surface; however, a large number of crystal particles will have identical reflections, and some of those reflections will be able to satisfy brags's law. The interplanner spacing, denoted by d, can be determined by first determining the values of λ and θ.

4.1.2 Lattice constant

Lattice constant defines the unit cell of a crystal. It is the length of one edge of the cell or an angle forming between edges. It can also be termed as lattice constant or lattice parameter. The distance, which is constant, between the lattice points is known as lattice constant. Following equation is used to calculate lattice constant.

In the below equation, lattice constant is "a", the wavelength of X-ray radiation is 1.54060Å for Cukα, miller indices are "h, k, l" and diffraction angle is θ.

4.1.3 Crystallite size

For the identification and confirmation of the experimentally obtained diffraction pattern it is compared to JCPDS cards. The structural properties are greatly influenced by particle size. According to Debay Sherrer equation, which is used to calculate particle size, crystal size is inversely proportional to peak width. So, the small crystallite size is related to peak broadening in XRD analysis. The Debay sherrer equation is used to calculate particle size.

4.1.4 X-Ray density

The X-ray diffraction data can be used for the calculation of sample material"s density [49]. If the lattice constant is known for each sample following formula will be used. Where ε represents molecular weight of sample, N is the Avogadro"s number (6.03×10^{23}) and "a" is the lattice constant. Eight formula units are possessed by each cell.

4.1.5 Bulk density

The intrinsic properties of materials define the bulk density or measured density. The density formula is generally used for the density calculation.

Where m represents the mass, r represents the radius; h is the thickness of the pressed pellet sample. For the calculation of measured density, a circular pallet of mass "m" is made using hydraulic press. Vernier caliper is used for measuring thickness and

radius of pallet and analytical balance is used for measuring mass of the pallet. The measured parameters are substituted in equation for the resultant density calculation.

4.1.6   Porosity fraction

Along with the alternation in compositions, the increase in the porosity fraction is observed. Following formula is used for calculation of porosity fraction.

4.2   Scanning electron microscopy

Scanning electron microscopy is an imaging technique which makes use of high energy electron beams for imaging Nano and bulk surfaces. When the highly energetic beam strikes the sample surface it provides following information.

- Composition of the sample.

- Phase mapping

- Topography of the sample.

When the beam hits the surface of material there will be various kind of interactions and signals are emitted as a result of these interactions such as transmitted electrons, back scattered electrons, secondary electrons, cathodoluminescence and characteristic X-rays [45].

4.2.1   Basic principle of SEM

When a specimen is subjected to high-energy electron beam irradiation, various signals are generated as a result of interactions between incident electrons and the constituent atoms of the specimen. These interactions are depicted in the figure that follows.[50]
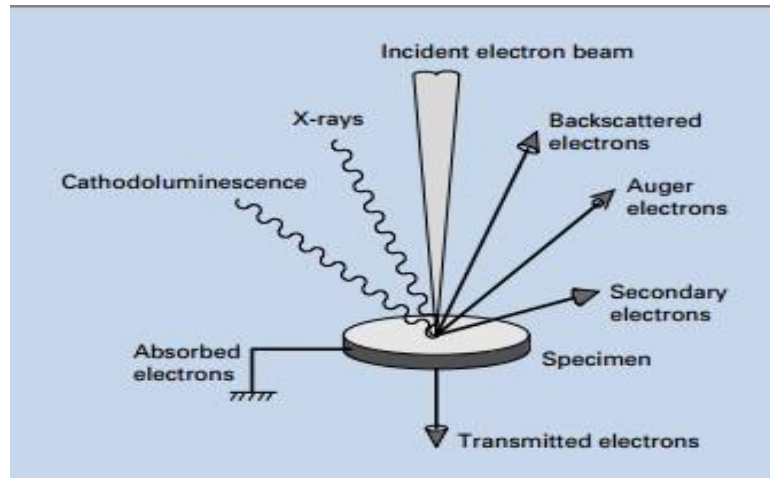
Figure 4.3: Emission of various electrons and EM waves from the specimen.[50]

Two classes of electron-matter interactions exist. that are:

- **Elastic scattering** – the electron trajectory within the specimen changes, but its kinetic energy and velocity remains essentially constant. The result is generation of backscattered electrons (BSE).

- **Inelastic scattering**– Inelastic scattering occurs when there is an interaction that causes loss of energy of the incident primary electron. Inelastically scattered electrons have a longer wavelength i.e

  - Secondary electrons

  - Phonon excitation i.e heating

  - Cathodoluminescence (visible light fluorescence)

  - Characteristic radiation (X-Ray)

  - Auger electrons (ejection of outer shell electrons low energetic)

4.2.2 Preparation of SEM samples

SEM is used for the study of surface morphology and for getting 3D images of surface. A very small amount of powdered material was dispersed in water using

ultrasonicate for about one hour and then drop of the mixture dripped onto a clean substrate. On substrate surface powder particles are dried and dispersed for further processed of analysis by SEM.

4.3   FTIR

The absorption, emission spectra ‟s, Raman scattering, and photoconductivity of the material can be obtained by using this analytical technique. The stretching modes of the elements present in composite and chemical purity of the sample can be determined using FTIR. It is known as FTIR because it involves the Fourier, a mathematical term. It collects the data from spectrum of matter. FTIR is used to determine the amount of light that a sample absorbs at a specific wavelength.

4.3.1   Working principle of FTIR

Infrared light from a polychromatic source fall on splitters in FTIR. The fixed mirror receives half of the incident light, while the moving mirror receives the other half. Transmitted light pass through the sample. The information about molecular component and structure of the sample can be obtained by interaction of light with sample. [51]
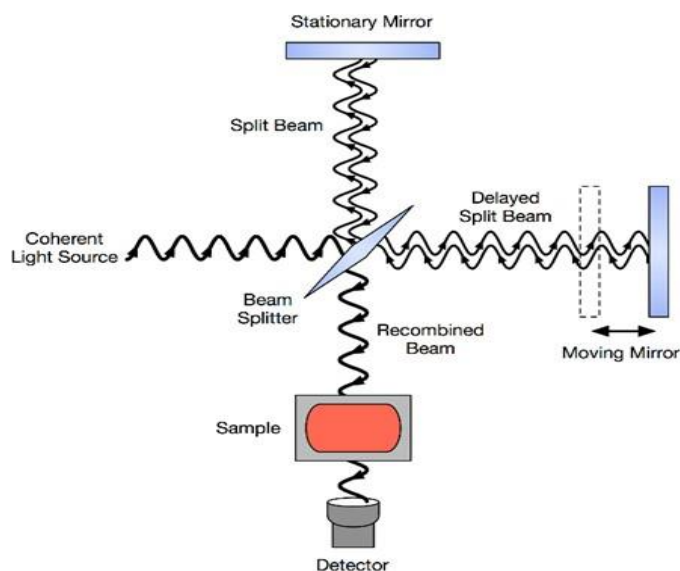

Figure 4.4: Schematic shows working principal of FTIR [52]

4.3.2 Applications of FTIR

- Gas chromatography is a technique for separating the constituents of a mixture from one another

- The analysis of liquid chromatography fraction can be done using FTIR.

- Tiny samples can be checked with the help of infrared microscope in sample chamber.

- FTIR is used to obtain the sample's emitted light spectrum rather than a light spectrum obtained through the sample.

4.3.3 Preparation of FTIR samples

KBr pellet method was for sample preparation because alkali salts give no absorption in IR spectrum. "Potassium salt (KBr) was placed in oven at 100 °C for one hour for removal of moisture. Small amount of sample and KBr was taken and ground to fine powder and pellet was prepared using pellet die set and Hydraulic press.

Mixture of ground KBr and sample was added into the die, and it was then placed into the press and with a pumping movement, moved the hydraulic pump handle downward until it shows 3 tons on the scale. Waited for 45 seconds, pressure was released, and die was taken out. Finally, a thin sample pellet having thickness in the range of 2-3 mm and diameter of ~13 mm was obtained.

4.4 Zeta Potential

The surface charge of nanoparticles was evaluated through the application of Zeta Potential using a Nano ZS Zetasizer (Zeta V2.3.2.19799 SN: ZPA220901). 2mg of samples of different concentrations were prepared in 200 ml of Ethanol at pH value of 6 at MEDIUM resolution.

The PEG-6000 (polyethylene-glycol) was dissolved in 6 mL of deionized (DI) water with continuous stirring at 50 °C for 40 min, 5mg of different concentration (5%, 10%, 15%, 20%, 25%) of Mg-doped CFNPs were added in 495ul of DI water.
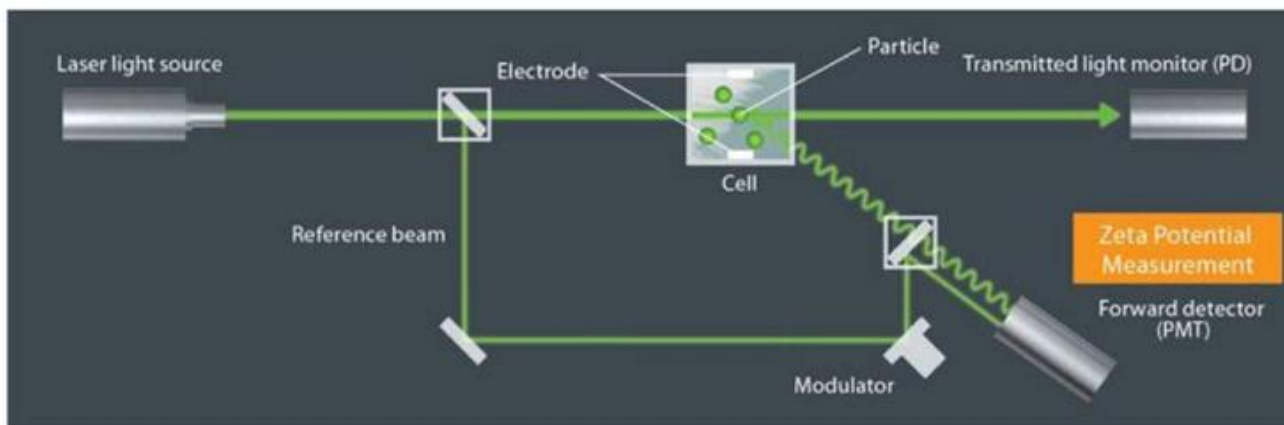
Figure 4.5: Encapsulation of Letrozole and PEG with Mg-doped CFNPs

Mg-doped CFNPs were mixed with PEG in 1:1 ratio, the solution was then placed in shaking incubator at 37 ˚C and 100 rpm for 2 hours. After 2 hours, the solution was subjected to centrifugation at 10,000 rpm for 10 minutes. The supernatant was removed, and DI water was added for washing purpose to remove excess coating.

Drug solution was made by adding 7 mL of ethanol as a solvent in 7 mg of Letrozole. The drug solution was then added to the PEG-coated Mg-doped CFNPs solution in a weight ratio of 1:1. The mixture of PEG-coated Mg-doped CFNPs and Letrozole was kept in shaking incubator at 37 ˚C and 100 rpm for 48 hours for the drug to load.

After loading the drug, PEG-coated Mg-doped CFNPs were separated by centrifugation at 10,000 rpm for 20 min and rinsed with DI water 5 times to collect all free drug in supernatant. The supernatant was removed and DI water was added to the drug encapsulated NPs [20].

The supernatant containing unloaded drug molecules was examined by UV-Visible absorption spectroscopy at 250 nm. The drug loading efficiency of the NPs was calculated using the following equation.

$$\text{Drug loading } (\%) = \frac{\text{initial drug weight} - \text{supernatent drug weight}}{\text{intial drug weight}} \times 100$$
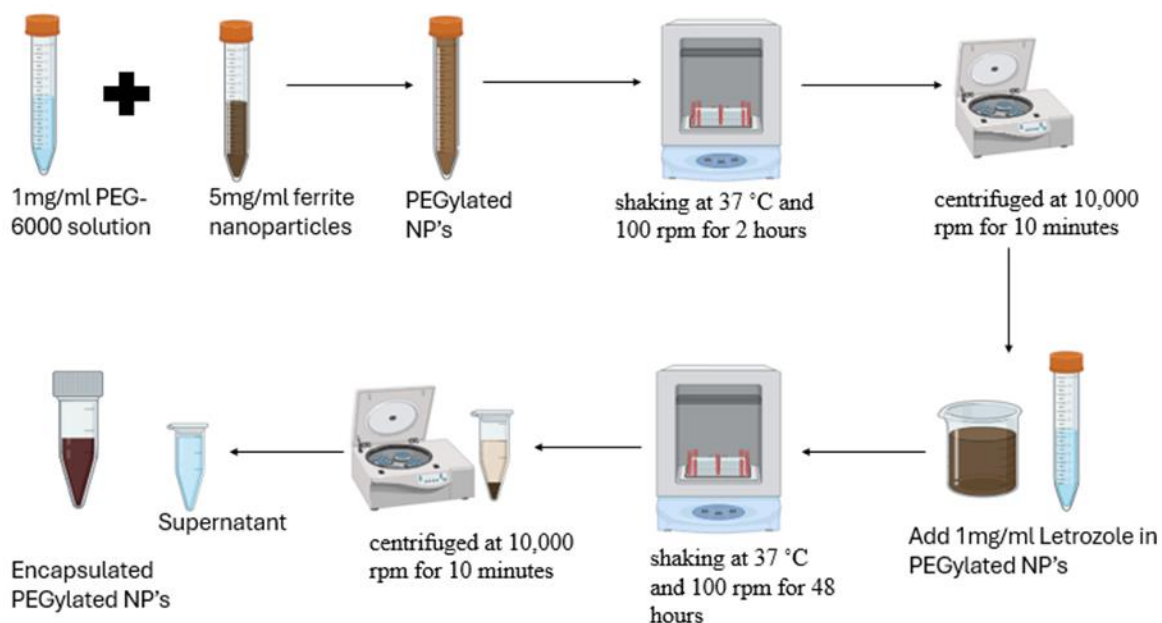
Figure 4.6: Encapsulation of Letrozole and PEG with Mg-doped CFNPs

4.5   Drug Release Assay

Drug release assay of Letrozole encapsulated PEGylated Mg-doped CFNPs was carried out by Sample and Separate method. To conduct the drug release assay, the initial step involves the construction of the standard curve for Letrozole. To achieve this, varying concentrations of Letrozole were prepared. A stock solution containing 1mg/1ml of Letrozole in ethanol was made. Subsequently, dilutions of 30 μg/ml, 25μg/ml, 20μg/ml, 15μg/ml, 10μg/ml, and 5μg/ml were prepared from this stock solution. The resulting dilutions were then analyzed using UV/Vis absorption spectroscopy at a wavelength of 240nm, and the standard curve was plotted.

4.5.1   In vitro Drug Release Assay of Mg-doped CFNPs

The drug release of Letrozole from PEGylated Mg-doped CFNPs was observed through the addition of 50 ml of phosphate-buffered saline (PBS) to a solution containing 0.0915 mg/ml of NPs. The dispersion of the drug-loaded ferrite NPs into the PBS solution was achieved by subjecting it to continuous stirring at 100 rpm in a shaking incubator. At

various time intervals of 2 h, 4 h, 6 h, 8 h, and 10 h, 2 ml of the solution was extracted for spectroscopy analysis at 240 nm. To maintain the original volume of 50 ml, an equivalent amount of fresh PBS was added after each extraction. The experiment was repeated in triplicates**.**

4.6   Hemolytic Assay Mg-doped CFNPs

The evaluation of the hemolytic activity of Letrozole loaded PEGylated Mg-doped CFNPs was conducted by means of a hemolysis assay, as documented in a previous study [21] . To commence the experiment, fresh human blood was collected and placed in an EDTA tube. Subsequently, the blood underwent centrifugation for a duration of 10 minutes at a speed of 10,000 rpm in order to obtain the supernatant.
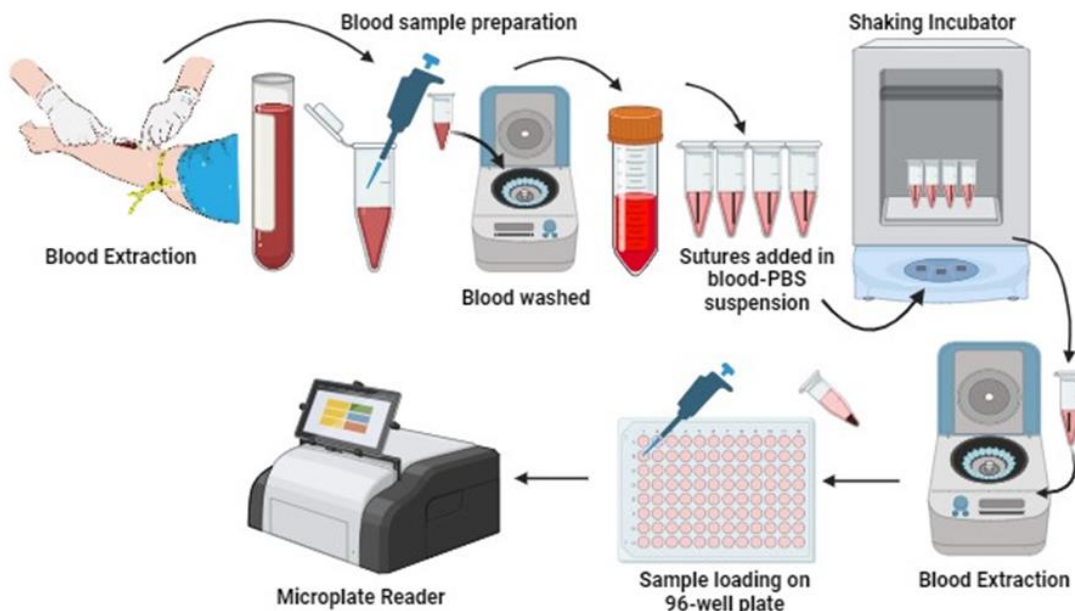

Figure 4.7: Hemolytic assay to evaluate biocompatibility of mg doped cobalt ferrite nanoparticles.

This particular procedure was repeated a total of five times, employing PBS at a pH level of 7.4, thus yielding a pure pellet. The subsequent step involved the addition of

five different concentrations of Mg-doped CFNPs (5%, 10%, 15%, 20%, 25%) to the blood sample, while simultaneously adjusting the final volume to 1 mL using PBS. The resulting samples were subsequently placed in in a shaking incubator for 4 hours, with the incubator set to a speed of 80 rpm. Following this incubation period, the samples were subjected to centrifugation for 10 minutes at a speed of 5000 rpm, and the absorbance of the supernatant collected was measured at a wavelength of 540 nm in triplicates. In order to establish positive and negative controls, Triton-X-100 and blood samples in PBS were employed, respectively. The percentage of hemolytic activity was calculated using the equation mentioned below.

$$hemolysis\ (\%) = \frac{Absorption\ Sample - Absorption\ Negative\ Control}{Absorption\ Positive\ Control - Negative\ Control} \times 100$$

4.7   MTT Assay Mg-doped CFNPs

3-(4,5-dimethyl-2-thiazolyl)-2,5-diphenyl-2H-tetrazolium bromide (MTT) was purchased from Sigma-Aldrich, USA. Solvents such as phosphate buffer saline, ethanol (99%), DMEM media, penicillin−streptomycin (10,000 U/mL), and fetal bovine serum (FBS) were purchased from Fisher Scientific, UK.

MTT assay is a cell viability assay that is used to analyze the biocompatibility of nanoparticles and other drugs on different cell lines. We perform our calculations according to IC50 value of Letrozole for MCF-7 (86.5nM) and for MDA-MB-231 (178.3nM). HEK293, MCF-7 and MDA-MB-231 (ATCC HTB-26) cells were cultivated in DMEM supplemented with 1% of penicillin−streptomycin and 10% FBS. For MTT Assay, Cells were incubated at 37 °C under 95% moisturized air with 5% CO2. Before the experiment, cells were trypsinized (0.25% Trypsin and EDTA) and seeded (1×104 cells/well) (counted using Equations 3 & 4) on 96-well plates with flat bottom wells.

The cells were incubated with Bare Mg-doped CFNPs, PEGylated Mg-doped CFNPs, and Letrozole conjugated PEGylated Mg-doped CFNPs with various concentrations for 48hrs to analyze cell viability using 10µl (5 mg/mL) MTT solution (3-4 hr incubation) followed by the addition of 100 µl DMSO to dissolve formazan crystals

for recording absorbance in microplate reader at 570nm. For MTT assay results evaluation following formula was used (Equation 5):

$$\text{Media required for plating} = \text{No of squares counted} \times \frac{1 \times 10^4 cells}{\text{ml}} \div$$

$$Total\ counted\ cells$$

$$C_1V_1 = C_2V_2$$

$$\text{Cell viability }(\%) = \frac{Sample\ Absorbance - Blank\ Absorbance}{Control\ Absorbance - Blank\ Absorbance} \times 100$$
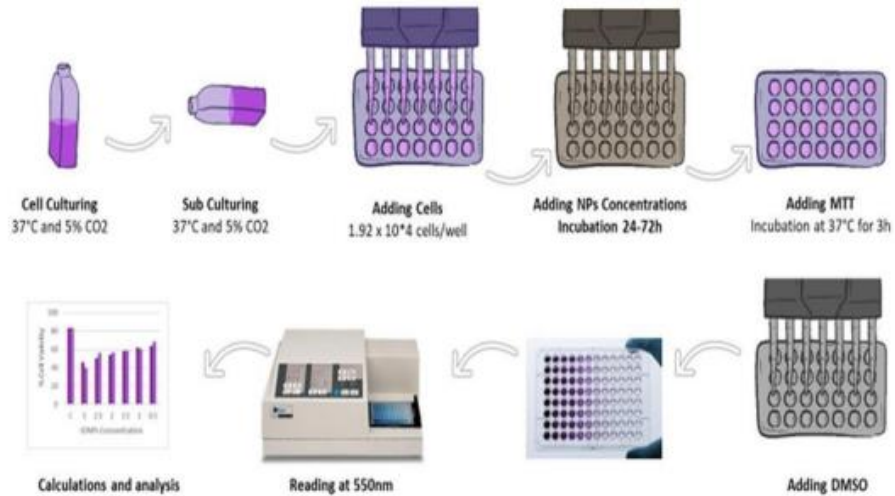

Figure 4.8: MTT Assay Protocol for cell viability analysis of ferrite nanoparticels

CHAPTER 5:   RESULTS AND DISCUSSION

5.1   XRD (X-ray diffraction) results

The XRD analysis is widely used to determine the phase structure, lattice parameters and crystallite size of crystalline solids. The XRD patterns were obtained at room temperature within an angle range of 20°-80° (2θ) with Cu—Kα (1.5406 Å) radiation. Mg-doped cobalt ferrites ($Co_{1-x}Mg_xFe_2O_4$ x=0.0, 0.05, 0.10, 0.15, 0.20, 0.25) samples were calcinated at 800^0C for 3 hours before XRD analysis to obtain fine powder.

The obtained peak patterns were used for the identification and measurement of different structural phases and parameters. Figure 3 shows sharp crystalline peaks of Mg-doped CFNPs that can be witnessed for different ferrite samples. The XRD peaks are classified (220), (311), (400), (511) and (440) for 30.10°, 35.45°, 43.09°, 56.97° and 62.54° respectively.

All the peaks of the cubic crystal system corresponding to space group Fd-3m were indexed with the standard pattern for MgFe2O4 reported in JCPDS No (00-003-0864). The lattice constant has been calculated using the unit cell calculator software which employs the formula:

$$\frac{1}{d^2} = \frac{h^2 + k^2 + l^2}{a^2}$$

where d is the interplanar spacing, (h k l) are the miler indices, and a is the lattice constant. The crystallite size is also calculated using Debye Scherrer's formula which is 32nm [23].

$$t = \frac{k\lambda}{\beta cos\theta}$$

Where β is the full-width peak at half maximum (in radians) at the observed peak angle 2θ, k is the crystallite shape factor (considered as 0.94) and λ is the wavelength of X-ray.
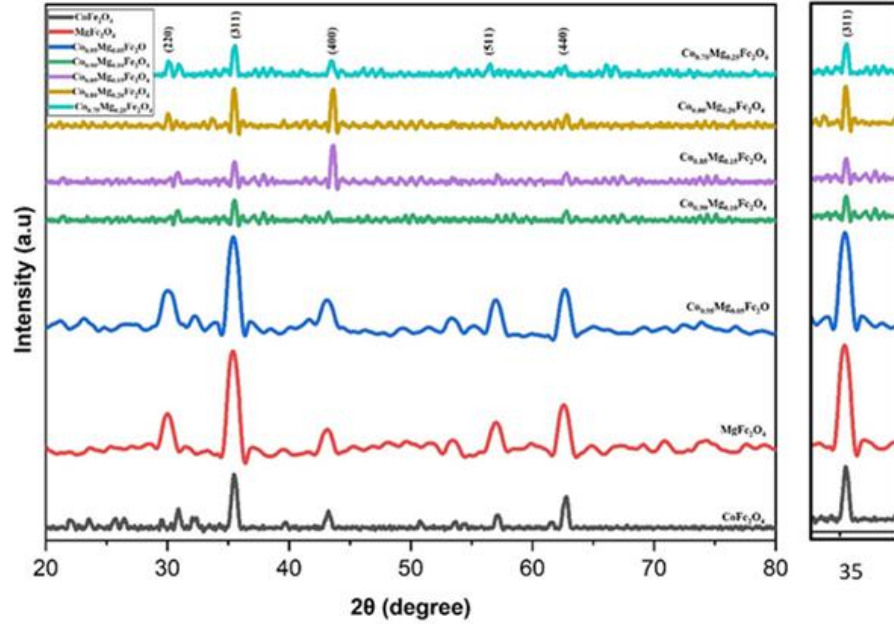

Figure 5.1: XRD spectra of Mg-doped CFNPs

5.2 Scanning electron microscopy (SEM) analysis

The SEM images show the surface morphology of the synthesized cobalt ferrite magnetic nanoparticles (CMNF). The nanoparticles are dispersed throughout the sample and have an approximate spherical (cubic) size. 33 nm is the average particle size estimated from SEM images (Figure 4a), which is more in line with the size estimated from XRD data. Figure 4b shows that the Mg-doped CFNPs aggregated due to insufficient sonication time, which resulted to poor particle separation. Additionally, the primary particles were bound together by weak surface interactions, such as the Vander Waals force. Particle agglomeration and irregular morphology, which lack regular shapes, appear to be evidence for the gel formation that occurs when the solution is heated; these characteristics additionally appear in the calcined samples.
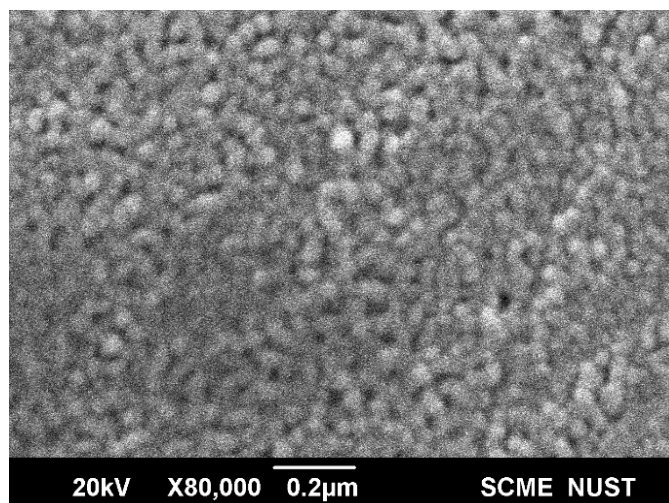
Figure 5.2: SEM image of CoFe2O4 nanoparticles
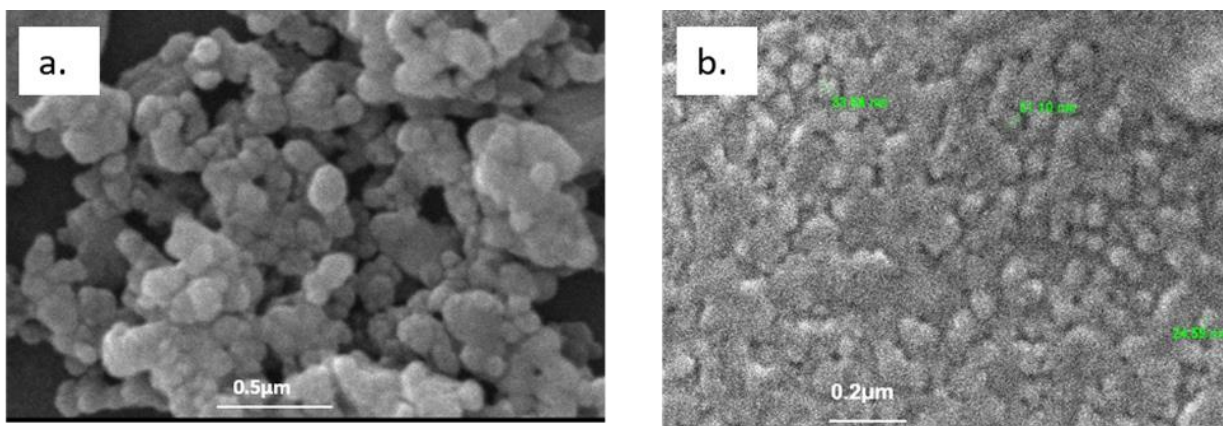
Figure 5.3: SEM images of Mg-doped CFNPs

5.3   EDX analysis

The EDX spectral analysis of the synthesized $CoFe_2O_4$ and Mg-doped cobalt ferrites ($Co_{1-x}Mg_xFe_2O_4$ are illustrated in Figure 5(a) and 5(b) respectively.

The percentage of EDX peaks represents the expected elemental composition of nanoparticles which confirms the presence of nanoparticles containing Co, Fe and O in Figure 5(a) and Co, Mg, Fe and O in Figure 5(b) as well. And no other impurity is found in synthesized nanoparticles.

Figure 5.4: (a). EDX results of $CoFe_2O_4$

5.4 FT-IR Spectroscopy

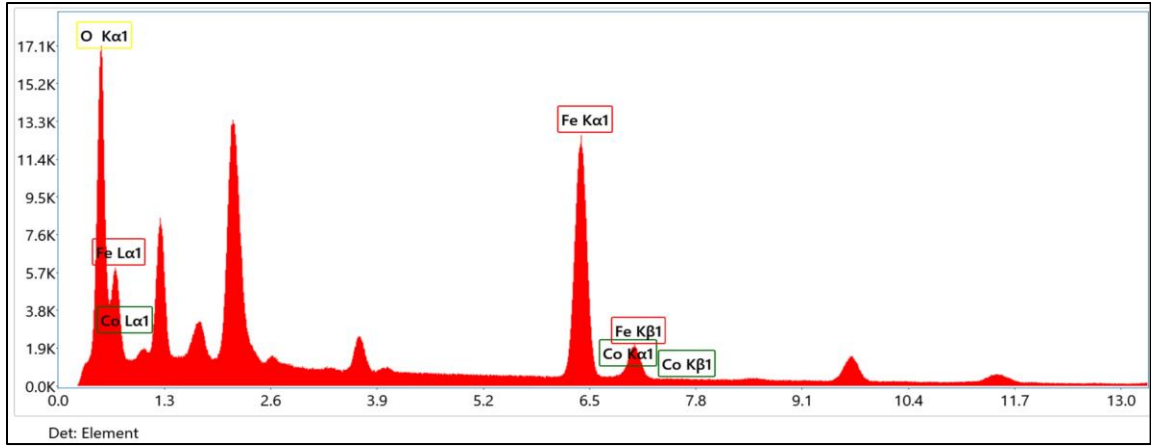It is common practice to examine the structure of a multi-component system using FTIR spectra. The spinel structure's formation and cationic distribution were confirmed with the room temperature $(25–27^0C)$.
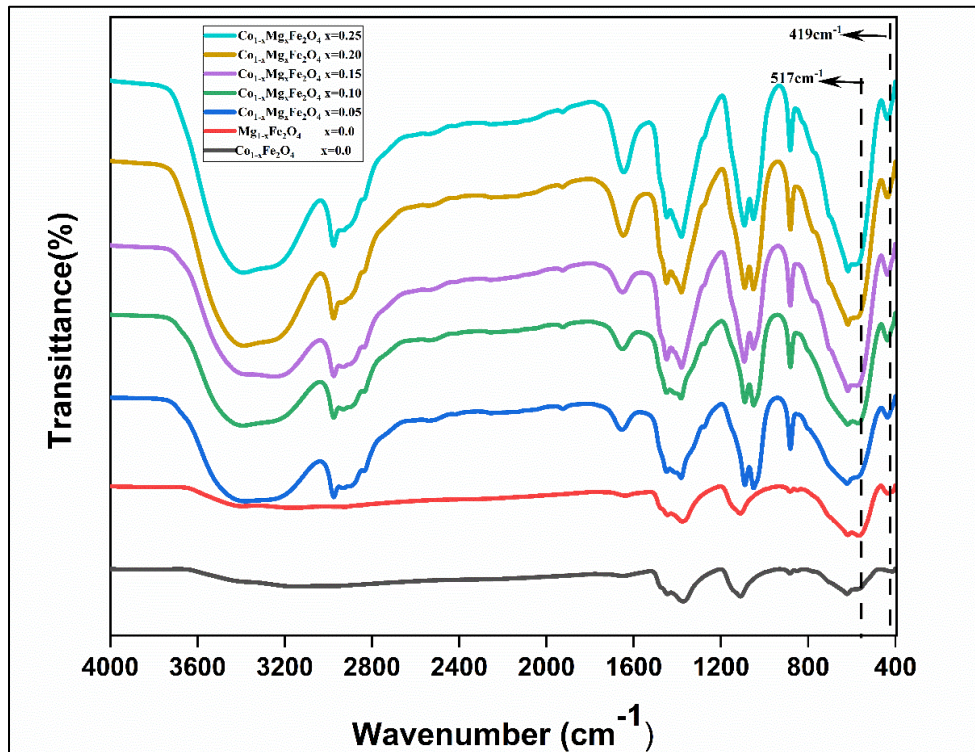

Figure 5.5: FTIR Spectra of Mg-doped CFNPs

Figure 2 the FTIR spectra of each sample of Mg-doped CFNPs that were measured in the 400–4000 cm^{-1} wave number range [22]. The formation of the spinel phase in all samples is indicated by the presence of two typical peaks in the FTIR spectra of all compositions. Stretching vibrations of octahedral site complexes (metal cation and oxygen) are observed at 419 cm^{-1} with the intense, while tetrahedral complexes are responsible for the peak at about 571 cm^{-1}.

5.5 Zeta Potential

The effective electric charge on the surface of the nanoparticle is quantified by the zeta potential. The concentration of ions with the opposite charge close to the nanoparticle surface screens out charges when a nanoparticle has a net surface charge [24]. The potential difference between the bulk fluid in which a particle is dispersed and the fluid layer containing the ions that are oppositely charged and connected to the nanoparticle surface is measured by the zeta potential. The zeta potential's magnitude yields particle stability information.
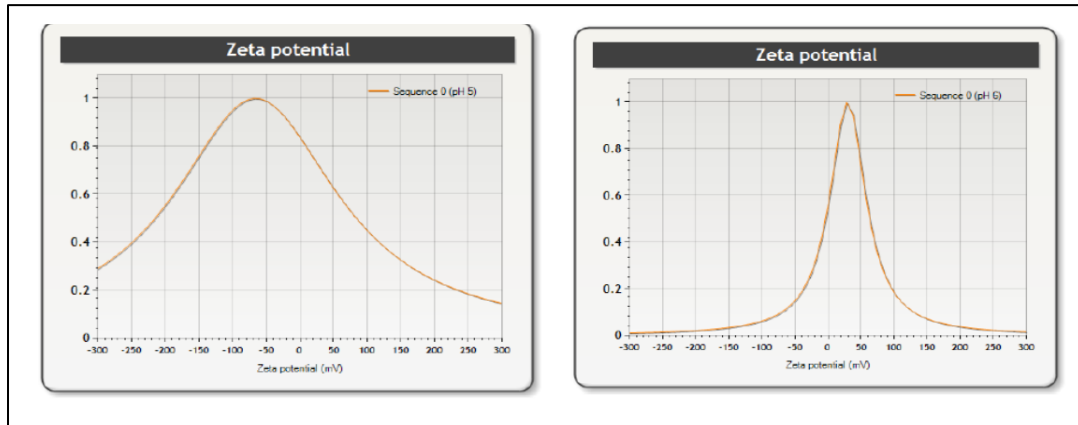
Figure 5.6: Zeta Potential of Mg-doped CFNPs

Higher potential magnitudes show greater electrostatic repulsion and, consequently, greater stability. The zeta potential of the nanoparticle's measures lower around or less than −28 mV, so we can confirm that the particles are agglomerated. The zeta potential of Mg-doped CFNPs was calculated and results was compared with change in concentration of Mg with in cobalt ferrites [25]. Zeta potential measures show a surface

charge of -13.3 mV, indicating a substantial number of negative charges on the surface of CoFe2O4 NP that contribute to the stability of NP (Figure 6).

5.6   Drug Release Profile

5.6.1   Drug Loading Efficiency

To find the % of Drug loading of the Letrozole conjugated PEGylated Mg-doped CFNPs, the standard curve of Letrozole was generated. Figure 7 shows the different concentration of Letrozole at 240nm was measured using UV visible spectroscopy [26]. The drug loading efficiency of the NPs can be calculated by using equation Eq. (1).

$$Drug\ loading(\%) = \frac{(\text{initial drug weight} - \text{supernatant drug weight}}{\text{inital drug weight}} \times 100$$

$$\text{Drug loading } (\%) = \frac{(1000\mu g - 2.88.56\mu g}{1000\mu g} \times 100$$
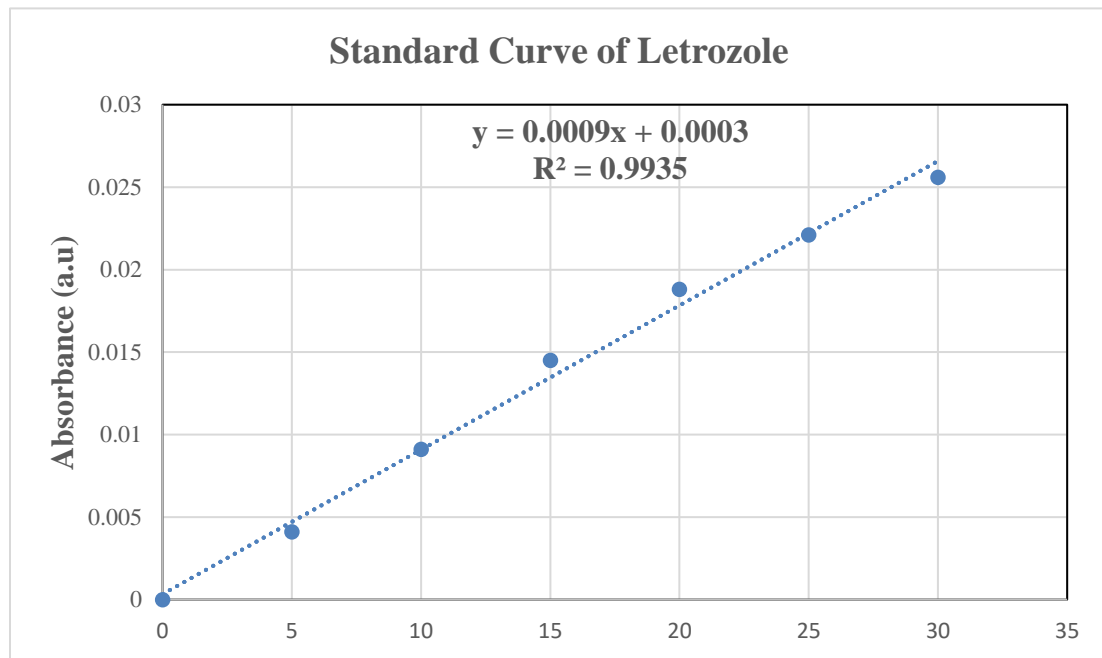
$$\text{Drug loading } (\%) = 71.15\%$$

Figure 5.7: Standard curve of Letrozole

48

5.6.2 *In vitro Drug Release Assay of Letrozole encapsulated Mg-doped CFNPs*

The drug release assay of PEGylated Mg-doped CFNPs was conducted and the results are depicted in Figure 8. As observed, all release profiles exhibit a first-order release kinetics, which is indicative of a diffusion process [27]. Initially, there was an exponential rise in the drug release, which continued for the first 10 hours for all five concentrations (5%,10%,15%,20%,25%). Highest drug release was observed in NPs with the greatest concentration of Mg (25%). The three profiles vary in that as the magnesium content rises, so does the total amount of drug released.
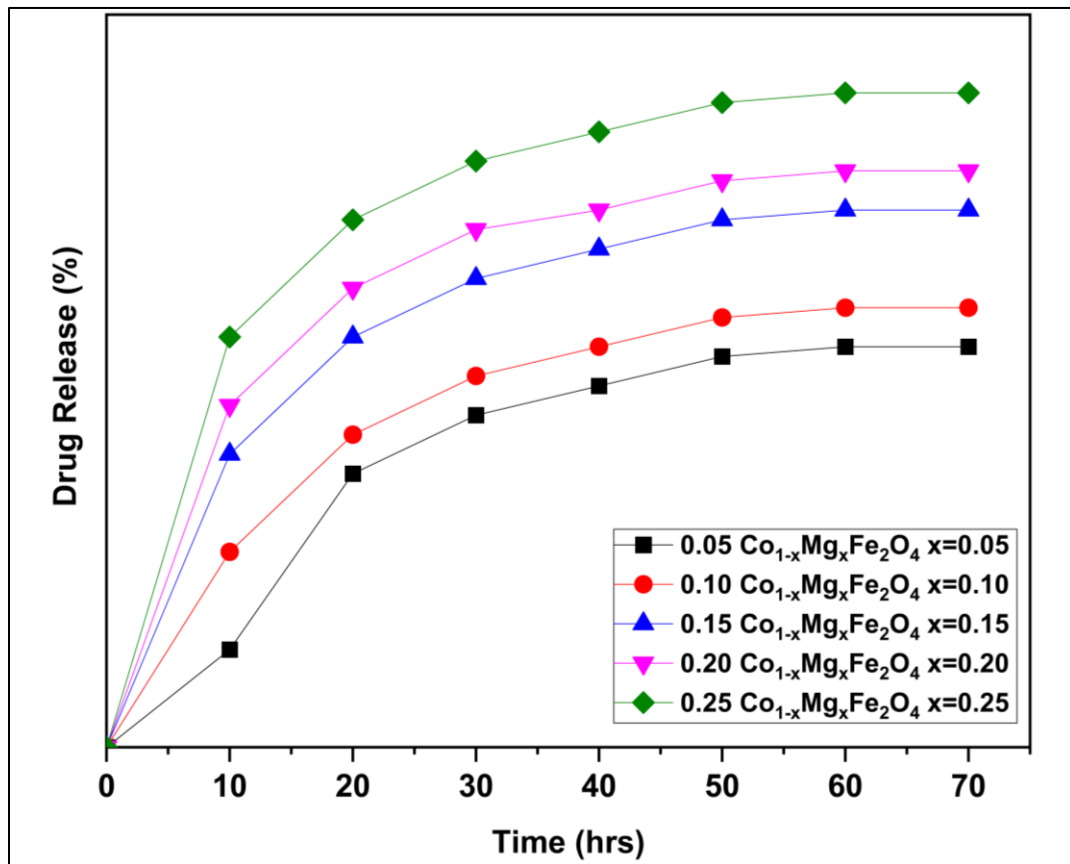

Figure 5.8: Drug release profile of Mg-doped CFNPs.

5.7 Hemolysis of Mg-doped CFNPs

The assessment of PEGylated Mg-doped CFNPs' capacity to lyse RBCs was performed using a hemolytic assay. This process involves the destruction of RBC

membranes and the release of internal components, which is attributed to the lysis of RBCs. In this assay, bare Mg-doped CFNPs were employed at five different concentrations (5%, 10%, 15%, 20%, and 25%), as depicted in Figure 9.

The results revealed that the hemolytic activity of Mg-doped CFNPs decreased with an increase in the concentration of magnesium. After 1 hour, the hemolytic activity of Mg-doped CFNPs at the highest concentration of Mg (25%) was found to be around 1.985% as compared to 2.41% hemolysis shown by NPs with Mg at lowest concentration (5%).

Based on ISO/TR 7406 standard, hemolytic rates of less than 5% are typically classified as nonhemolytic, which indicates that Mg-doped CFNPs are well beyond safe to be used as drug carriers [28].
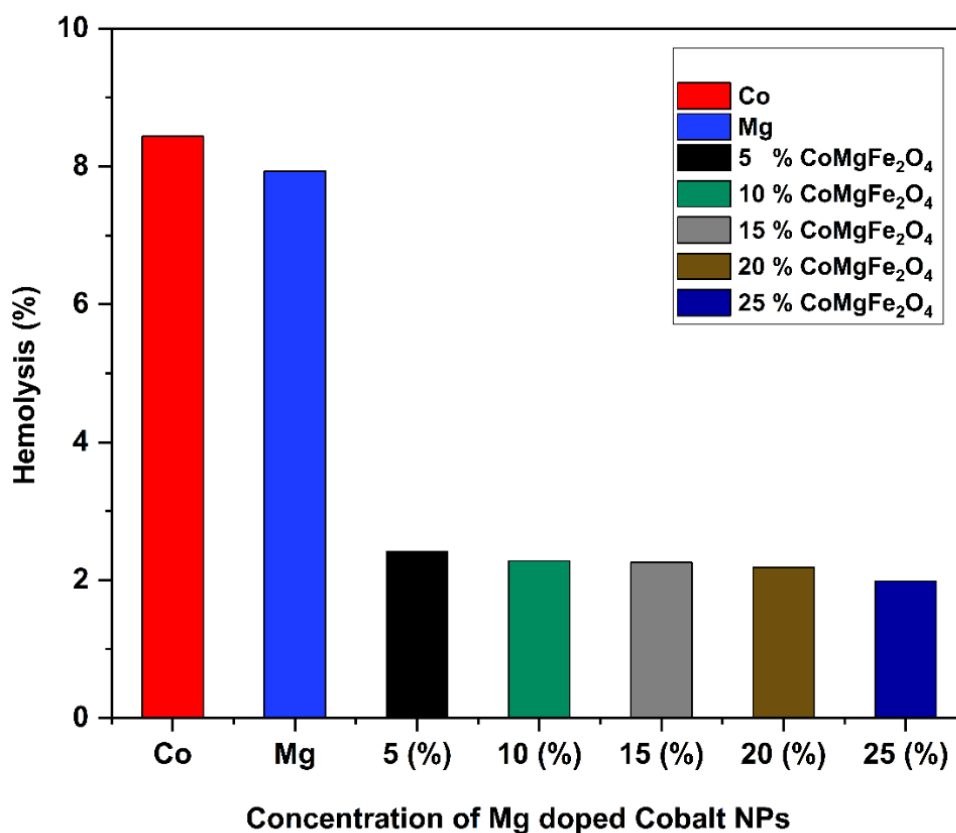

Figure 5.9: Hemolytic activity of Mg-doped CFNPs at different concentrations.

5.8   MTT Assay of Mg-doped CFNPs

The cytotoxicity of ferrite NPs at different concentrations was evaluated using the MTT assay in normal Human Embryonic Kidney (HEK) 293 cell lines, breast epithelial estrogen receptor-positive cell lines (MCF-7), and triple-negative breast cancer cells (MDA-MB-231).

These cell lines were tested with different concentrations of nanoparticles (5%,10%,15%,20%,25%,100% Co and 100% Mg). The common trend observed in Figure 10 suggests that the percentage cell viability decreased with increasing concentration of magnesium-doped cobalt Letrozole-conjugated nanoparticles.

At the highest concentration, the percentage cell viability was 70% for HEK-293 (Figure 10), 55% for MCF-7 (Figure 11), and 60% for MDA-MB-231 (Figure 12) cell lines. The cell viability percentage was the highest for PEGylated nanoparticles, indicating that PEG coating decreases the toxicity of bare nanoparticles and is safe to use as confirmed by previous studies [29].

The results showed that the percentage cell viability was higher in HEK-293 cell lines than in the other two cell lines (MCF-7) and (MDA-MB-231), indicating that there is no significant effect of ferrite nanoparticles on healthy cells.

Thus, it can be concluded that mildly doped cobalt ferrite nanoparticles are safe for use as drug carriers. The drug-conjugated PEGylated nanoparticles showed significantly lower cell viability in the MCF-7 cell line (Figure 11) and MDA-MB-231.

(Figure 12) than in HEK-293 cells, indicating that more cancer cells were killed. Drug-conjugated PEGylated nanoparticles in MCF-7 cells showed greater cytotoxicity towards breast cancer cells than MDA-MB-231 cells because MCF-7 cells are estrogen (ER)-positive receptors, whereas MDA-MB-231 is a triple-negative receptor.

Basically, Letrozole is commonly used to treat estrogen receptor positive breast cancer, as it specifically targets the hormone-dependent pathways that promote the growth of these tumors [30]. It is not typically used for the treatment of estrogen receptor-negative

breast cancer cells that's why it shows significant results in MCF-7 as compared to MDA-MB-231.

Figure 5.10: comparison of cytotoxicity of different concentration of Bare ferrite NPs, PEGylated NPs, Letrozole conjugated PEGylated NPs and Letrozole Drug on HEK 293 cell line.

Figure 5.11: Comparison of cytotoxicity of different concentration of Bare ferrite NPs, PEGylated NPs, Letrozole Conjugated PEGylated Nanoparticles and Letrozole drug on MCF-7 cell line.

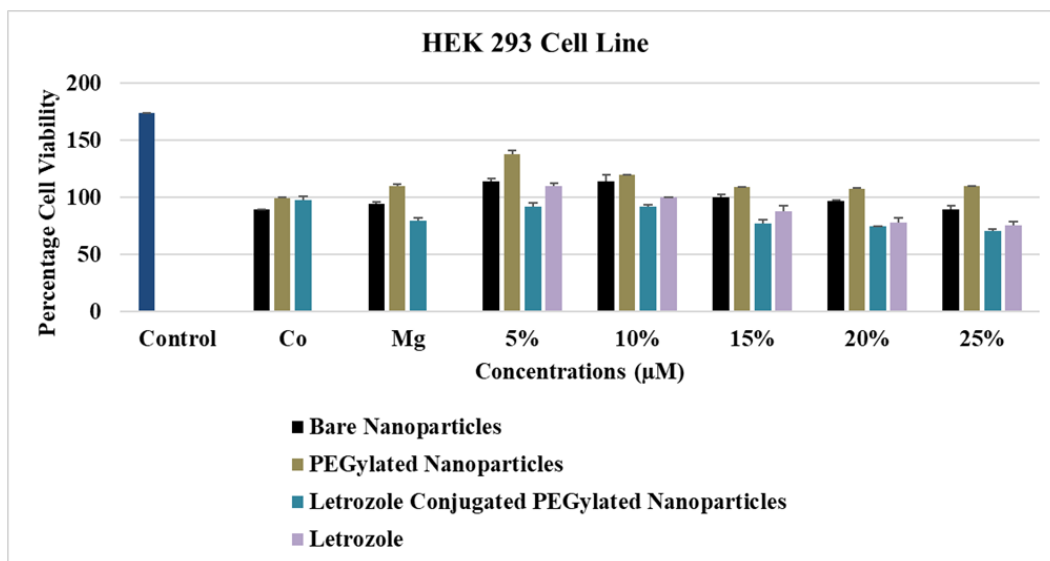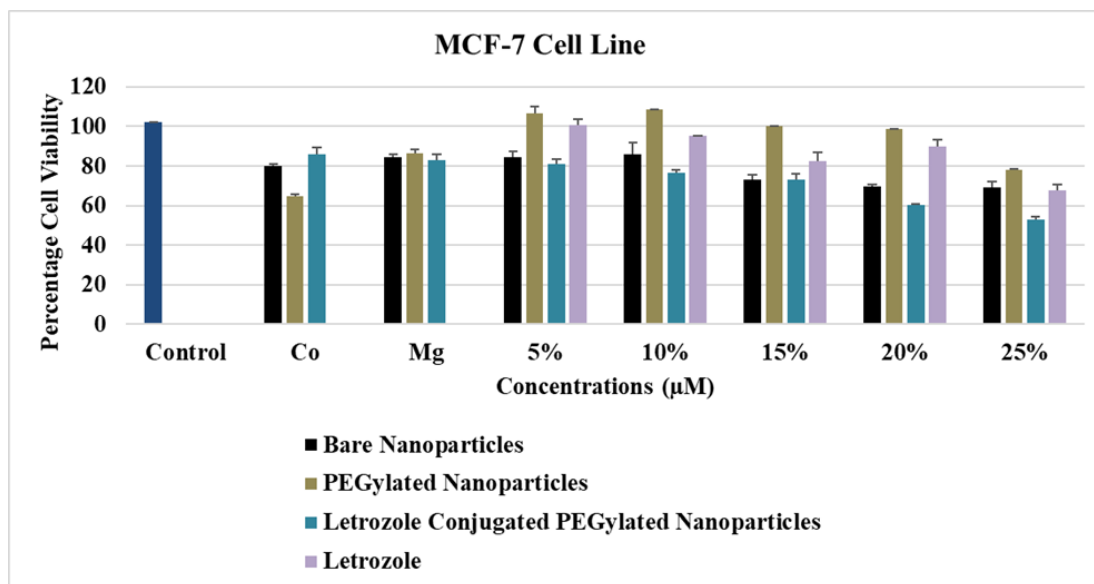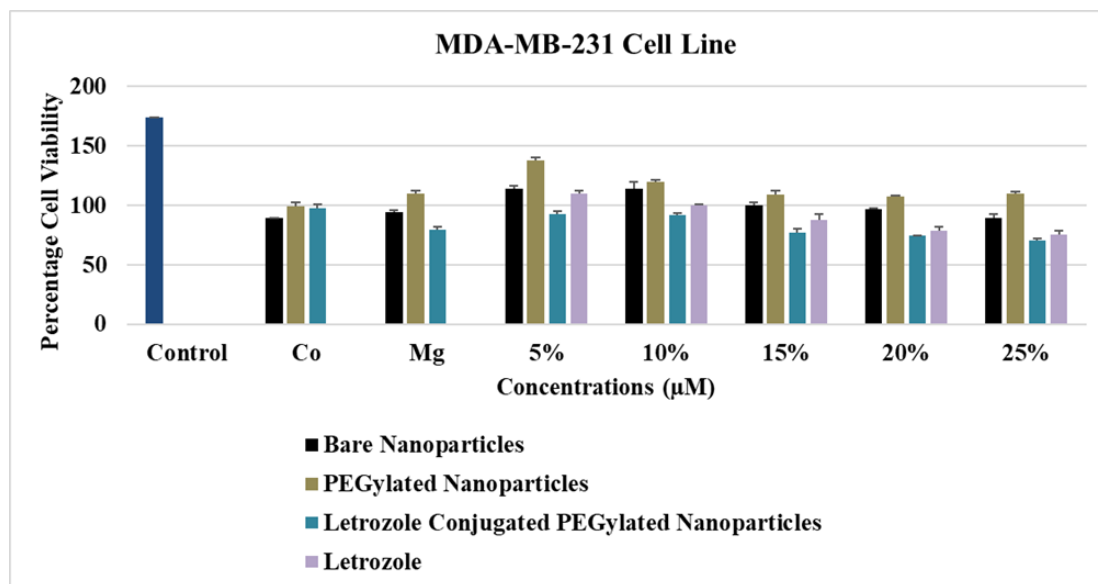**Figure 5.12:** comparison of cytotoxicity of different concentration of Bare ferrite NPs, PEGylated NPs, Letrozole Conjugated PEGylated Nanoparticles and Letrozole drug on MDA-MB-231 cell line.

CHAPTER 6: CONCLUSIONS AND FUTURE RECOMMENDATION

6.1   Conclusion

Mg-doped CFNPs with a composition of Co1-xMgxFe2O4 (where x= 0, 0.05, 0.10, 0.15, 0.20, and 0.25) were successfully synthesized through the sol-gel method using citric acid as the fuel. The Mg-doped CFNPs formed a cubic spinel structure and had an irregular morphology with crystallite sizes varying from 29 to 49 nm. FTIR spectroscopy confirmed the formation of two metallic bands and the stretching vibrations of octahedral (419 cm-1) and tetrahedral (571 cm-1) site complexes. SEM revealed the spherical nanoparticles with some degree of clustering and agglomeration. Based on the EDX spectra, Co, Fe, and O were present in CoFe2O4, and Co, Mg, Fe, and O were present in Co1-xMgxFe2O4. The synthesized Mg-doped CFNPs showed excellent magnetic properties and their application in biomedical field show that Mg-doped CFNPs show best hemolytic activity (<10%), drug release and cytotoxicity at the highest concentration of 0.25 and prevail to decrease the cell viability by about 55% on MCF-7 breast cancer cell line and 60% on MDA-MB-231 breast cancer cell line. The doping of cobalt ferrite with magnesium resulted in improved efficiency and decreased toxicity compared to the use of CoFe2O4 and MgFe2O4 individually. Furthermore, the results showed that these nanoparticles at specific concentrations were safe for targeted drug delivery.

6.2   Future Recommendations

Such a nanohybrid can absorb electromagnetic spectrum, so the studies of their microwave absorption as well as UV-Vis characterization can relate to important data which can be deployed for military applications. Often, to make the polymer blends somewhat conductive, different metallic media are added using various polymerization techniques. It's only natural that the next step regarding this research would be to add such a nanohybrid in a polymer matrix to study the mechanical as well as microwave properties of such an advanced hybrid. Owing to their enhanced dielectric properties, such a nanohybrid can be used in batteries cathode as well as in the construction of aerospace parts by incorporation of thermoset resins rendering them high stiffness and

strength even at very high temperatures. With the advancement in the field of composites and their versatile use in various industries, such a hybrid can revolutionize the field of nanoscience as well as nanotechnology , pushing the boundaries in the real of magnetism , dielectric , optical and electromagnetic application, biosensing , in vivo testing and other biomedical applications.

REFERENCES

1. ul, I., et al., Structural, magnetic and electrical properties of Co1− xZnxFe2O4 synthesized by co-precipitation method. Journal of magnetism and magnetic materials, 2007. **311**(2): p. 494-499.

2. Djurberg, C., et al., Dynamics of an interacting particle system: evidence of critical slowing down. Physical review letters, 1997. **79**(25): p. 5154.

3. Bradford, P., The aggregation of iron oxide nanoparticles in magnetic fields. 2012, University of Birmingham.

4. Iacovacci, V., et al., Magnetic Field-Based Technologies for Lab-on-a-Chip Applications, in Lab-on-a-Chip Fabrication and Application. 2016, InTech.

5. Flinn, R.A.et al. Engineering materials and their applications. Engineering Materials and Their Applications, 4th Edition, by Richard A. Flinn, Paul K. Trojan, pp. 1056. ISBN 0-471-12508-3. Wiley-VCH, December 1994., 1994: p. 1056.

6. Hilpert, S.et al. phsik. Ges, 1909. **11**: p. 293.

7. Snoek, J.et al, Magnetic and electrical properties of the binary systems MO. Fe2O3. Physica, 1936. **3**(6): p. 463-483.

8. Néel, L,et al. Antiferromagnetism and ferrimagnetism. Proceedings of the Physical Society. Section A, 1952. **65**(11): p. 869.

9. Koops, C,et al. On the dispersion of resistivity and dielectric constant of some semiconductors at audiofrequencies. Physical Review, 1951. **83**(1): p. 121.

10. Chen, C.-W,et al. Magnetism and metallurgy of soft magnetic materials. 2013: Courier Corporation.

11. Yeadon, W.H.et al., Handbook of small electric motors. Vol. 1040. 2001: McGraw-Hill New York.

12. Bragg, W.H,et al. The structure of the spinel group of crystals. The London, Edinburgh, and Dublin Philosophical Magazine and Journal of Science, 1915. **30**(176): p. 305-315.

13. Gorter, E.W,et al. Saturation magnetization and crystal chemistry of ferrimagnetic oxides. I. II. Theory of ferrimagnetism. Philips Res. Rep., 1954. **9**: p. 295- 320,321-365.

14. Clarricoats,et al. Microwave ferrites. 1961: Wiley.

15. Barth, T.F,et al. Spinel structures: with and without variate atom equipoints. Zeitschrift für Kristallographie-Crystalline Materials, 1932. **82**(1-6): p. 325-341.

16. Structural and magnetic properties of zinc substituted Co 0.8 Mn 0.2 Fe 2 O 4 nanoparticles.

17. (Bhandare et al. 2020)Mittal, V., et al., Cation distribution in NixMg1− xFe2O4 studied by XPS and Mössbauer spectroscopy. Solid state communications, 2006. **137**(1-2): p. 6-10.

18. Amer, M., et al., Mössbauer, Infrared and X-ray Studies for Ni_ {0.5} Zn_ {0.5} Cr_xFe_ {2-x} O_4 Ferrites. Turkish Journal of Physics, 2005. **29**(3): p. 163-177.

19. Brockhouse, B., BN Brockhouse, LM Corliss, and JM Hastings, Phys. Rev. 98, 1721 (1955). Phys. Rev., 1955. **98**: p. 1721.

20. Nalbandian, L., et al., Hydrothermally prepared nanocrystalline Mn–Zn ferrites: synthesis and characterization. Microporous and Mesoporous Materials, 2008. **114**(1-3): p. 465-473.

21. Yáñez-Vilar, S., et al., A simple solvothermal synthesis of MFe2O4 (M= Mn, Co and Ni) nanoparticles. Journal of Solid State Chemistry, 2009. **182**(10): p. 2685-2690.

22. Xia, A. and H. Zhang, Effects of excessive Zn2+ ions on intrinsic magnetic and

structural properties of Ni0. 2Zn0. 6Cu0. 2Fe2O4 powder prepared by chemical coprecipitation method. Current Applied Physics, 2010. **10**(3): p. 825-827.

23.   Lerouge, F., G. Cerveau, and R.J. Corriu, Supramolecular self-organization in non-crystalline hybrid organic–inorganic nanomaterials induced by van der Waals interactions. New Journal of Chemistry, 2006. **30**(10): p. 1364-1376.

24.   Banerjee, A., et al., Catalytic activities of cobalt, nickel and copper ferrospinels for sulfuric acid decomposition: the high temperature step in the sulfur based thermochemical water splitting cycles. international journal of hydrogen energy, 2011. **36**(8): p. 4768-4780.

25.   Samoila, P., et al., The effect of chelating/combustion agent on catalytic activity and magnetic properties of Dy doped Ni–Zn ferrite. Materials Chemistry and Physics, 2012. **136**(1): p. 241-246.

26.   Druc, A., et al., Optimization of synthesis conditions and the study of magnetic and dielectric properties for MgFe2O4 ferrite. Open Chemistry, 2013. **11**(8): p. 1330-1342.

27.   Shirsath, S.E., et al., Chemical tuning of structure formation and combustion process in CoDy 0.1 Fe 1.9 O 4 nanoparticles: influence@ pH. Journal of nanoparticle research, 2013. **15**(10): p. 1976.

28.   Sulaiman, N., et al., Superparamagnetic calcium ferrite nanoparticles synthesized using a simple sol-gel method for targeted drug delivery. Bio-medical materials and engineering, 2015. **26**(s1): p. S103-S110.

29.   Jeseentharani, V., et al., Synthesis of metal ferrite (MFe2O4, M= Co, Cu, Mg, Ni, Zn) nanoparticles as humidity sensor materials. Journal of Experimental Nanoscience, 2013. **8**(3): p. 358-370.

30.   Mouli, K.C., T. Joseph, and K. Ramam, Synthesis and magnetic studies of Co-Ni-Zn ferrite nano crystals. Journal of nanoscience and nanotechnology, 2009. **9**(9): p. 5596-5599.

31. Özgür, Ü., Y. Alivov, and H. Morkoç, Microwave ferrites, part 1: fundamental properties. Journal of materials science: Materials in electronics, 2009. **20**(9): p. 789-834.

32. Gul, I., et al., Physical and magnetic characterization of co-precipitated nanosize Co–Ni ferrites. Scripta Materialia, 2007. **56**(6): p. 497-500.

33. Pradeep, A., P. Priyadharsini, and G. Chandrasekaran, Sol–gel route of synthesis of nanoparticles of MgFe2O4 and XRD, FTIR and VSM study. Journal of Magnetism and Magnetic Materials, 2008. **320**(21): p. 2774-2779.

34. Smitha, T., et al. Electrical and magnetic properties of nano-sized magnesium ferrite. in IOP Conference Series: Materials Science and Engineering. 2015. IOP Publishing.

35. BORTNIC, R.-A., et al., SYNTHESIS OF COBALT FERRITE NANOPARTICLES VIA A SOL-GEL COMBUSTION METHOD. Studia Universitatis Babes-Bolyai, Chemia, 2016. **61**(4).

36. Thankachan, S., et al., A comparative study of structural, electrical and magnetic properties of magnesium ferrite nanoparticles synthesised by sol-gel and co-precipitation techniques. Journal of experimental Nanoscience, 2013. **8**(3): p. 347-357.

37. Moradmard, H., et al., Structural, magnetic and dielectric properties of magnesium doped nickel ferrite nanoparticles. Journal of Alloys and Compounds, 2015. **650**: p. 116-122.

38. Mahalakshmi, S. and K.S. Manja, Ac electrical conductivity and dielectric behavior of nanophase nickel ferrites. Journal of Alloys and Compounds, 2008. **457**(1-2): p. 522-525.

39. Hashim, M., et al., Structural, Dielectric, AC Conductivity, and Magnetic Properties of Cr3+ Substituted Ni–Mg Ferrite Nanoparticles. Journal of Nanoengineering and Nanomanufacturing, 2013. **3**(1): p. 39-47.

40. Velhal, N.B., et al., Structural, dielectric and magnetic properties of nickel substituted cobalt ferrite nanoparticles: Effect of nickel concentration. AIP Advances, 2015. **5**(9): p. 097166.

41. (Velho-Pereira et al. 2015).

42. Bhise, R., S. Rathod, and A. Supekar, Dielectric, Magnetic, Electric and Structural Properties of Ni0. 2-Cox-Zn0. 8-x Ferrite Nanoparticles Synthesized bySol-Gel Auto Combustion Method. International Journal of Advancements inResearch & Technology,2013. **2**: p. 1-6.

43. (Gheidari et al. 2020).

44. Ali, A.A., et al., MWCNTs/carbon nano fibril composite papers for fuel cell and super capacitor applications. Journal of Electrostatics, 2015. **73**: p. 12-18.

45. (Velho-Pereira et al. 2015).

46. Melo, R., et al., Magnetic ferrites synthesised using the microwave-hydrothermal method. Journal of Magnetism and Magnetic Materials, 2015. **381**: p. 109-115.

47. Klug, H.P. and L.E. Alexander, X-ray diffraction procedures. 1954.

48. Özdemir, Z.G., et al., Super-capacitive behavior of carbon nano tube doped 11-(4-cyanobiphenyl-4-oxy) undecan-1-ol. Journal of Molecular Liquids, 2015. **211**: p. 442-447.

49. "Scanning Electron Microscope A to Z." N.p., n.d.W.N.

50. Zhang, X., et al., One-step solvothermal synthesis of graphene/Mn3O4 nanocomposites and their electrochemical properties for supercapacitors. Materials Letters, 2012. **68**: p. 336-339.

51. Ying, Y. and P. Yu, Microprobing Structural Architecture Using Mid-Infrared Vibrational Molecular Spectroscopy, in Applications of Molecular Spectroscopy to Current Research in the Chemical and Biological Sciences. 2016, InTech.

52. Murugesan, C., M. Perumal, and G. Chandrasekaran, Structural, dielectric and magnetic properties of cobalt ferrite prepared using auto combustion and ceramic route. Physica B: Condensed Matter, 2014. **448**: p. 53-56.

53. Mirzaee, S., S.F. Shayesteh, and S. Mahdavifar, Anisotropy investigation of cobalt ferrite nanoparticles embedded in polyvinyl alcohol matrix: a Monte Carlo study. Polymer, 2014. **55**(16): p. 3713-3719.

54. Rosnan, R., et al., Effects of Mg substitution on the structural and magnetic properties of Co0. 5Ni0. 5− x Mg x Fe2O4 nanoparticle ferrites. Chinese Physics B, 2016. **25**(4): p. 047501.

55. arma, M.C., et al., Estimating the Cation Distributions in Ferrites Using X-Ray, FT-IR, and Magnetization Measurements. Physics Research International, 2014. **2014**.

56. Naeem, M., et al., Structural, electrical and magnetic characterization of Ni–Mg spinel ferrites. Journal of Alloys and Compounds, 2009. **487**(1-2): p. 739-743.

57. Denton, A.R. and N.W. Ashcroft, Vegard"s law. Physical review A, 1991. **43**(6): p. 3161.

58. Reshak, A., Dispersion of the second harmonic generation in GaNxAs1− x (x= 0.25, 0.5, 0.75) alloys. Journal of Alloys and Compounds, 2014. **589**: p. 213-217.

59. Rao, C.N.R., Chemical applications of infrared spectroscopy. 1963, Academic Press.

60. Levin, M. and M. Miller, Maxwell's" Treatise on Electricity and Magnetism". Soviet Physics Uspekhi, 1981. **24**(11): p. 904.

61. Kumar, A., P. Sharma, and D. Varshney, Structural, vibrational and dielectric study of Ni doped spinel Co ferrites: Co1− xNixFe2O4 (x= 0.0, 0.5, 1.0). Ceramics International, 2014. **40**(8): p. 12855-12860.

62. Yadav, G., et al., Enhancement in Magnetic and Dielectric Properties of

Magnesium Ferrite by Lithium Substitution Applicable for High Frequency Shielding Material.

63.   Chandra, K., S. Singhal, and S. Goyal, Magnetic and Mössbauer spectral studies of nano crystalline cobalt substituted magnesium ferrites (Mg x Co 1− x Fe 2 O4), in ICAME 2007. 2008, Springer. p. 247-252.

64.   Sharma, J., et al., Dielectric properties of nanocrystalline Co-Mg ferrites. Journal of Alloys and Compounds, 2015. **649**: p. 362-367.

65.   Gabal, M., Y. Al Angari, and F. Al-Agel, Cr-substituted Ni–Zn ferrites via oxalate decomposition. Structural, electrical and magnetic properties. Journal of Magnetism and Magnetic Materials, 2015. **391**: p. 108-115.

66.   John, H., et al., Conducting polyaniline composites as microwave absorbers. Polymer composites, 2007. **28**(5): p. 588-592.

67.   Gul, I., et al., Optical, magnetic and electrical investigation of cobalt ferrite nanoparticles synthesized by co-precipitation route. Journal of alloys and compounds, 2010. **507**(1): p. 201-206.

68.   Kumari, N., V. Kumar, and S. Singh, Structural, dielectric and magnetic investigations on Al 3+ substituted Zn-ferrospinels. RSC Advances, 2015. **5**(47): p. 37925-37934.

69.   Cole, K.S. and R.H. Cole, Dispersion and absorption in dielectrics II. Direct current characteristics. The Journal of Chemical Physics, 1942. **10**(2): p. 98-105.

70.   Kumari, R., et al., Rietveld refinement, impedance spectroscopy and magnetic properties of Bi0. 8Sr0. 2FeO3 substituted Na0. 5Bi0. 5TiO3 ceramics. Journal of Magnetism and Magnetic Materials, 2016. **414**: p. 1-9.

71.   Ye, H., R.B. Jackman, and P. Hing, Spectroscopic impedance study of nanocrystalline diamond films. Journal of applied physics, 2003. **94**(12): p. 7878-

7882.

72.   Kaiser, M., Electrical conductivity and complex electric modulus of titanium doped nickel–zinc ferrites. Physica B: Condensed Matter, 2012. **407**(4): p. 606- 61.